

Chaotic von Zeipel-Lidov-Kozai oscillations of a binary system around a rotating supermassive black hole

Kei-ichi Maeda^{1,2}, Priti Gupta³, and Hirotada Okawa⁴

¹*Department of Physics, Waseda University, Shinjuku, Tokyo 169-8555, Japan*

²*Center for Gravitational Physics and Quantum Information, Yukawa Institute for Theoretical Physics, Kyoto University, 606-8502 Kyoto, Japan*

³*Department of Physics, Indian Institute of Science, Bangalore 560012, India*

⁴*Waseda Institute for Advanced Study (WIAS), 1-21-1 Nishi Waseda, Shinjuku-ku, Tokyo 169-0051, Japan*



(Received 4 October 2023; accepted 13 November 2023; published 27 December 2023)

In this paper, we investigate the dynamics of a binary system that orbits a rotating supermassive black hole. Our approach employs Fermi-Walker transport to construct a local inertial reference frame, and to set up a Newtonian binary system. We consider a scenario in which a circular geodesic observer is positioned around a Kerr black hole, and thereby derive the equations of motion governing the binary system. To eliminate the interaction terms between the c.m. of the binary and its relative coordinates, we introduce a small acceleration for the observer. This adjustment leads to the c.m. closely following the observer's orbit, deviating from a circular geodesic. Here, we first focus on elucidating the stability conditions in a hierarchical triple system. Subsequently, we discuss the phenomenon of von Zeipel-Lidov-Kozai oscillations, which manifest when the binary system is compact and the initial inclination exceeds a critical angle. In hard binary systems, these oscillations exhibit regular behavior, while in soft binary systems, they exhibit a chaotic character, characterized by irregular periods and amplitudes, albeit remaining stable. Additionally, we observe an orbital flip under circumstances of large initial inclination. As for the motion of the c.m., we observe deviations from a purely circular orbit that transform into stable yet chaotic oscillations characterized by minute amplitude variations.

DOI: [10.1103/PhysRevD.108.123041](https://doi.org/10.1103/PhysRevD.108.123041)

I. INTRODUCTION

In the wake of the groundbreaking discovery of gravitational waves (GWs) by the LIGO-Virgo-KAGRA (LVK) Collaboration [1,2], the fields of astronomy and physics have embarked on an unprecedented journey. These detections have ushered in a new era, reshaping our comprehension of celestial phenomena in profound ways. One remarkable outcome has been the identification of astrophysical entities characterized by their astonishingly massive stellar-mass black holes (BHs) [3]. The synergy between gravitational wave observations and electromagnetic counterparts has provided further compelling evidence affirming Einstein's general theory of relativity, as we have observed that the speed of GWs is consistent with the speed of light [4]. The increase in detections anticipated in the coming decade offers an opportunity to probe fundamental questions of the utmost significance—testing of theories of gravity under the strong field regimes. Additionally, unraveling the redshift distribution of black holes (BHs) and their surrounding environments holds great promise [5–9]. To utilize the potential of detections, it is imperative to accurately model the anticipated GW waveforms.

While current observations from LVK Collaboration predominantly emanate from isolated binary systems, it

is crucial to remain open to the possibility that nature may unveil more intricate sources. Since there have been studies suggesting the presence of a hierarchical triple formation channel [10,11], our focus turns towards the examination of three-body systems. Within the densely populated environs surrounding supermassive black holes (SMBHs) in galactic nuclei, it is conceivable that binary systems may give rise to natural hierarchical triple systems [12–17]. Recent compelling evidence from LIGO events has hinted at the possibility that hierarchical systems could serve as a prominent formation channel for the merging binary BHs [11,18,19]. In light of these developments, this paper explores the dynamics within such hierarchical triple systems, shedding light on their potential as sources of gravitational wave signals.

In a hierarchical triple, the distance between two bodies (forming an “inner” binary) is much less than the distance to the third body. von Zeipel was the first one to explore the dynamics of restricted hierarchical triples in 1910, revealing a remarkable phenomenon [20], and in 1962, Lidov and Kozai independently rediscovered the same [21,22], [known as von Zeipel-Lidov-Kozai (vZLK) resonance]—when the two orbits are inclined relative to each other, there is a periodic exchange between orbital

eccentricity and relative inclination in secular timescale [23]. This phenomenon can excite the eccentricity close to unity, in turn, giving rise to the high emission of GWs lying in the observable band of future space-based detectors. While the eccentricity will most likely decay upon entering the frequency band of ground-based detectors, it may boost the number of detections if the dominant formation channel is hierarchical mergers [24].

There has been extensive work on dynamics of such systems based on Newtonian or post-Newtonian approximation [25–32]. Indirect observation of GW from a triple system is also studied by analyzing the cumulative shift of periastron time of a binary pulsar undergoing vZLK oscillations [33,34]. The presence of a heavier tertiary has been considered in previous studies [35,36] using double-averaged equations of motion to investigate relativistic effects such as de-Sitter and Lense-Thirring precessions. An additional study also investigated 3-body PN (3BpN) secular effect in a hierarchical system with heavy third body using a multiple scale method [37]. As well, they pointed out that 3BpN effects affected the evolution of these triples, resulting in a wider range of eccentricity and inclination. Some research studies explore the impact of supermassive black hole spin on nearby binary black hole systems. SMBH spin (Lense-Thirring precession and gravitomagnetic force in particular) affects binary black hole (BBH) eccentricity and orbital inclination, potentially altering BBH merger times [38,39]. Furthermore, in recent years, substantial interest has been directed toward three-body systems and their gravitational wave emissions [40–51]. In the context of a triple system with a massive tertiary component, the vZLK timescale is significantly reduced to just a few years, enhancing the gravitational observations' potential to capture recurrent gravitational waves arising from vZLK oscillations [48,50].

In our approach, we consider a binary system orbiting an SMBH and the binary is treated as perturbations of SMBH spacetime. When dealing with a single object orbiting the SMBH, it can be regarded as a test particle, subject to the gravitational influence of the central black hole. However, the dynamics become notably more intricate in the case of a binary system because the self-gravitational mutual interaction is much stronger than the gravitational tidal force by SMBH. In order to analyze such a hierarchical system, we first prepare a local inertial frame and set up a binary in this frame. When a binary is tightly bounded but the mutual gravitational interaction is not so strong, the binary motion can be discussed by Newtonian gravitational dynamics.

Using Fermi normal coordinate system or Fermi-Walker transport, we can construct a local inertial frame [52–54]. Using such a technique, there are several discussions on a tidal force acting on stars near SMBH [55–58], and a few works on a binary system have been discussed [59–61]. In the previous paper, assuming that SMBH is described by a spherically symmetric Schwarzschild spacetime, we

analyze dynamics of such a system in detail [62]. We showed that the vZLK oscillations appear even near the innermost stable circular orbit (ISCO) radius when a binary is compact enough and the inclination angle is larger than the critical value. Although the oscillations are regular for a highly compact binary, when a binary is softer, we find the chaotic vZLK oscillations, i.e., the oscillations become irregular both in the oscillation period and in the amplitude. Especially, if the initial inclination is large, we find an orbital flip of the relative inclination of the inner and outer orbits. However SMBH may be rotating in nature. Hence in this paper, we extend our analysis into a rotating Kerr SMBH.

The paper is organized as follows: We summarize our method discussed in the previous paper, which can be applied to any background spacetime, in Sec. II. In Sec. III, assuming an observer moving along a circular geodesic in Kerr black hole, we derive the equations of motion for a binary system. We also discuss the interaction terms between the c.m. of a binary and its relative coordinates. Introducing small acceleration of an observer, we remove the interaction terms, finding the equations of motion for the c.m., which gives small deviations from a circular geodesic. In Sec. IV, for our numerical analysis, we rewrite the equations of motion in dimensionless form, introduce the orbital parameters for analysis, and show how to prepare the initial data. In Sec. VA, we analyze many models numerically to find the stability conditions for a hierarchical triple system. We then show the properties of binary motions such as the vZLK oscillations, chaotic features, and orbital flips. A summary and discussion follow in Sec. VI. In Appendix A, we solve motions of the c.m. of a binary and show its stability. We also present the Lagrange planetary equations of the model and write down the equations for the orbital parameters of a binary taking averages over inner and outer binary cycles in Appendix B. We show that this simplified method recovers numerical results obtained by direct integration of the equations of motion in the case of a hard binary. It also provides the vZLK oscillation timescale and the maximum and minimum values of eccentricity.

Notation used: Greek letters range from 0 to 3, while Roman letters run from 1 to 3; Hatted indices denote tetrad components in a proper reference frame rotating along an observer; Bar over symbols correspond to quantities in a static tetrad frame. We use $G = c = 1$ unless specified otherwise.

II. BINARY SYSTEM IN A CURVED SPACETIME

We first summarize how to calculate a binary motion near a supermassive black hole (SMBH), which was described in details in paper I [62]. We discuss a binary system in a fixed curved background. A binary consists of two point particles with the masses m_1 and m_2 . In order to solve a binary motion around SMBH, we set up a local

inertial frame [52,63], and then put a self-gravitating binary system, which follows approximately Newtonian dynamics in a local inertial frame [59].

A. Proper reference frame

The background spacetime metric, which describes an SMBH, is given by $d\bar{s}^2 = \bar{g}_{\mu\nu} dx^\mu dx^\nu$. We consider an observer, whose orbit is given by a world line γ described by $x^\mu = z^\mu(\tau)$, where τ is a proper time of the observer. The 4-velocity of the observer is given by $u^\mu(\tau) \equiv dz^\mu/d\tau$.

We then prepare an orthonormal tetrad system $\{e_{\hat{\alpha}}^\mu\}$ along γ , which is defined by the conditions such that $e_{\hat{\alpha}}^\mu e_{\hat{\beta}\mu} = \eta_{\hat{\alpha}\hat{\beta}}$, $e_{\hat{0}}^\mu = u^\mu$, where $\eta_{\hat{\alpha}\hat{\beta}}$ is Minkowski spacetime metric.

For a given 4-velocity u^μ , this tetrad system is determined up to three-dimensional rotations. The tetrad $e_{\hat{\alpha}}^\mu$ is transported along γ as

$$\frac{De_{\hat{\alpha}}^\mu}{d\tau} = -(a^\mu u^\nu - u^\mu a^\nu + u_\alpha \omega_\beta \epsilon^{\alpha\beta\mu\nu}) e_{\hat{\alpha}\nu},$$

where $a^\mu \equiv Du^\mu/d\tau$ and ω_μ are the acceleration of the observer and the angular velocity of a rotating spatial basis vector $e_{\hat{\alpha}}^\mu$, respectively.

Next, we construct a local coordinate system (the observer's proper reference system) near the world line γ , which is described as $(x^{\hat{\alpha}}) = (c\tau, x^{\hat{\alpha}})$, where the spatial components $x^{\hat{\alpha}}$ is measured from the point at τ on the world line γ along the spatial hypersurface $\Sigma(\tau)$ perpendicular to γ .

The metric form of this proper reference frame up to the second order of $x^{\hat{\alpha}}$ is given by

$$g_{\hat{\mu}\hat{\nu}} = \eta_{\hat{\mu}\hat{\nu}} + \varepsilon_{\hat{\mu}\hat{\nu}} + O(|x^{\hat{\alpha}}|^3), \quad (2.1)$$

where

$$\varepsilon_{\hat{0}\hat{0}} = -\frac{1}{c^2} \left[2a_{\hat{k}} x^{\hat{k}} + (c^2 \bar{\mathcal{R}}_{\hat{0}\hat{k}\hat{0}\hat{\rho}} - \omega_{\hat{j}\hat{k}} \omega_{\hat{\rho}}^{\hat{j}}) x^{\hat{k}} x^{\hat{\rho}} + \frac{(a_{\hat{k}} x^{\hat{k}})^2}{c^2} \right], \quad (2.2)$$

$$\varepsilon_{\hat{0}\hat{j}} = -\frac{1}{c^2} \left[c\omega_{\hat{j}\hat{k}} x^{\hat{k}} + \frac{2}{3} c^2 \bar{\mathcal{R}}_{\hat{0}\hat{k}\hat{j}\hat{\rho}} x^{\hat{k}} x^{\hat{\rho}} \right], \quad (2.3)$$

$$\varepsilon_{\hat{j}\hat{j}} = -\frac{1}{c^2} \left[\frac{1}{3} c^2 \bar{\mathcal{R}}_{\hat{i}\hat{k}\hat{j}\hat{\rho}} x^{\hat{k}} x^{\hat{\rho}} \right], \quad (2.4)$$

with $\bar{\mathcal{R}}_{\hat{\mu}\hat{\nu}\hat{\rho}\hat{\sigma}}$ being the tetrad component of the Riemann curvature of a background spacetime and $\omega_{\hat{j}\hat{k}} \equiv \varepsilon_{\hat{j}\hat{k}} \omega^{\hat{\rho}}$ [52,59,63].

The acceleration and angular frequency in the proper reference frame are defined by

$$\hat{a}^{\hat{j}} \equiv e_{\hat{\mu}}^{\hat{j}} \frac{Du^{\hat{\mu}}}{d\tau},$$

$$\hat{\omega}^{\hat{j}} \equiv \frac{1}{2} \epsilon^{(3)\hat{j}\hat{k}\hat{\rho}} e_{\hat{\rho}\mu} \frac{De_{\hat{k}}^\mu}{d\tau},$$

where $\epsilon^{(3)\hat{j}\hat{k}\hat{\rho}} \equiv e^{\hat{j}\nu} e^{\hat{k}\rho} e^{\hat{\rho}\sigma} u^\mu \epsilon_{\mu\nu\rho\sigma}$. If the observer's orbit is the geodesic, we recover the Fermi normal coordinates.

B. Self-gravitating binary system

Now we discuss a self-gravitating binary system in a fixed curved background spacetime [59]. We are interested in the case where Newtonian dynamics is valid in the observer's proper reference frame. The necessary condition is that the typical scale ℓ_{binary} of a binary system should satisfy

$$\ell_{\text{binary}} \ll \min \left[\frac{1}{|\hat{a}^{\hat{j}}|}, \frac{1}{|\hat{\omega}^{\hat{j}}|}, \ell_{\bar{\mathcal{R}}} \right],$$

where $\ell_{\bar{\mathcal{R}}}$ is the minimum curvature radius defined by

$$\ell_{\bar{\mathcal{R}}} \equiv \min [|\bar{\mathcal{R}}_{\hat{\mu}\hat{\nu}\hat{\rho}\hat{\sigma}}|^{-\frac{1}{2}}, |\bar{\mathcal{R}}_{\hat{\mu}\hat{\nu}\hat{\rho}\hat{\sigma};\hat{\alpha}}|^{-\frac{1}{3}}, |\bar{\mathcal{R}}_{\hat{\mu}\hat{\nu}\hat{\rho}\hat{\sigma};\hat{\alpha};\hat{\beta}}|^{-\frac{1}{4}}].$$

A gravitational interaction in a self-gravitating binary system can be described by the metric deviation from a local Minkowski spacetime. For example, to discuss Newtonian dynamics of particle 1, it is enough to consider the 00 component of the metric perturbation, $\varphi_{\hat{0}\hat{0}}^{(1)} = -2\Phi^{(1)}/c^2$, where $\Phi^{(1)}$ is the Newtonian potential of particle 1, which is

$$\Phi^{(1)}(x^{\hat{i}}) = -\frac{Gm_2}{|x_1^{\hat{i}} - x_2^{\hat{i}}|}.$$

The equations of motion for particle 1 in the observer's proper reference frame can be derived by the variation with respect to $x_1^{\hat{i}}$ of the action

$$S^{(1)} = \int d\tau \mathcal{L}^{(1)},$$

where

$$\mathcal{L}^{(1)} \equiv -m_1 c \sqrt{-g_{\hat{\mu}\hat{\nu}}^{(1)} \frac{dx_1^{\hat{\mu}}}{d\tau} \frac{dx_1^{\hat{\nu}}}{d\tau}},$$

with the metric $g_{\hat{\mu}\hat{\nu}}^{(1)}$ given by

$$g_{\hat{\mu}\hat{\nu}}^{(1)} = \eta_{\hat{\mu}\hat{\nu}} + \varepsilon_{\hat{\mu}\hat{\nu}} + \varphi_{\hat{\mu}\hat{\nu}}^{(1)}. \quad (2.5)$$

We also find a similar action for particle 2. Next, we perform the post-Newtonian expansion of the total

Lagrangian $\mathcal{L} = \mathcal{L}^{(1)} + \mathcal{L}^{(2)}$. The Lagrangian for a binary up to 0.5 PN order is given by

$$\mathcal{L}_{\text{binary}} = \mathcal{L}_{\text{N}} + \mathcal{L}_{1/2}, \quad (2.6)$$

where

$$\mathcal{L}_{\text{N}} \equiv \frac{1}{2} \sum_{I=1}^2 m_I \dot{\mathbf{x}}_I^2 + \frac{Gm_1 m_2}{|\mathbf{x}_1 - \mathbf{x}_2|} + \mathcal{L}_a + \mathcal{L}_\omega + \mathcal{L}_{\bar{\mathcal{R}}}, \quad (2.7)$$

with

$$\begin{aligned} \mathcal{L}_a &= - \sum_{I=1}^2 m_I a_{\hat{k}} x_I^{\hat{k}}, \\ \mathcal{L}_\omega &= - \sum_{I=1}^2 m_I \left[\epsilon_{\hat{j}\hat{k}\hat{\ell}} \omega^{\hat{\ell}} x_I^{\hat{k}} \dot{x}_I^{\hat{j}} - \frac{1}{2} (\omega^2 x_I^2 - (\boldsymbol{\omega} \cdot \mathbf{x}_I)^2) \right], \\ \mathcal{L}_{\bar{\mathcal{R}}} &= - \frac{1}{2} \sum_{I=1}^2 m_I \bar{\mathcal{R}}_{\hat{0}\hat{k}\hat{\ell}} \dot{x}_I^{\hat{k}} \dot{x}_I^{\hat{\ell}}, \end{aligned}$$

and

$$\mathcal{L}_{1/2} \equiv - \frac{2}{3} \sum_{I=1}^2 m_I c^2 \bar{\mathcal{R}}_{\hat{0}\hat{k}\hat{j}\hat{\ell}} x_I^{\hat{k}} x_I^{\hat{\ell}} \frac{\dot{x}_I^{\hat{j}}}{c}. \quad (2.8)$$

A dot ($\dot{\cdot}$) denotes the proper time derivative $d/d\tau$.

Introducing the c.m. coordinates and the relative coordinates by

$$\begin{aligned} \mathbf{R} &= \frac{m_1 \mathbf{x}_1 + m_2 \mathbf{x}_2}{m_1 + m_2}, \\ \mathbf{r} &= \mathbf{x}_2 - \mathbf{x}_1, \end{aligned}$$

we find the Newtonian Lagrangian [Eq. (2.7)] in terms of \mathbf{R} and \mathbf{r} as

$$\mathcal{L}_{\text{N}} = \mathcal{L}_{\text{CM}}(\mathbf{R}, \dot{\mathbf{R}}) + \mathcal{L}_{\text{rel}}(\mathbf{r}, \dot{\mathbf{r}}), \quad (2.9)$$

where

$$\begin{aligned} \mathcal{L}_{\text{CM}}(\mathbf{R}, \dot{\mathbf{R}}) &= \frac{1}{2} (m_1 + m_2) \dot{\mathbf{R}}^2 + \mathcal{L}_{\text{CM-}a}(\mathbf{R}, \dot{\mathbf{R}}) \\ &\quad + \mathcal{L}_{\text{CM-}\omega}(\mathbf{R}, \dot{\mathbf{R}}) + \mathcal{L}_{\text{CM-}\bar{\mathcal{R}}}(\mathbf{R}, \dot{\mathbf{R}}), \end{aligned}$$

with

$$\begin{aligned} \mathcal{L}_{\text{CM-}a} &= -(m_1 + m_2) \mathbf{a} \cdot \mathbf{R}, \\ \mathcal{L}_{\text{CM-}\omega} &= -(m_1 + m_2) \left[\epsilon_{\hat{j}\hat{k}\hat{\ell}} \omega^{\hat{\ell}} \mathbf{R}^{\hat{k}} \dot{\mathbf{R}}^{\hat{j}} - \frac{1}{2} (\omega^2 \mathbf{R}^2 - (\boldsymbol{\omega} \cdot \mathbf{R})^2) \right], \\ \mathcal{L}_{\text{CM-}\bar{\mathcal{R}}} &= - \frac{1}{2} (m_1 + m_2) \bar{\mathcal{R}}_{\hat{0}\hat{k}\hat{\ell}} \mathbf{R}^{\hat{k}} \dot{\mathbf{R}}^{\hat{\ell}}, \end{aligned}$$

and

$$\mathcal{L}_{\text{rel}}(\mathbf{r}, \dot{\mathbf{r}}) = \frac{1}{2} \mu \dot{\mathbf{r}}^2 + \frac{Gm_1 m_2}{r} + \mathcal{L}_{\text{rel-}\omega}(\mathbf{r}, \dot{\mathbf{r}}) + \mathcal{L}_{\text{rel-}\bar{\mathcal{R}}}(\mathbf{r}, \dot{\mathbf{r}}),$$

with

$$\begin{aligned} \mathcal{L}_{\text{rel-}\omega} &= -\mu \left[\epsilon_{\hat{j}\hat{k}\hat{\ell}} \omega^{\hat{\ell}} r^{\hat{k}} \dot{r}^{\hat{j}} - \frac{1}{2} (\omega^2 r^2 - (\boldsymbol{\omega} \cdot \mathbf{r})^2) \right], \\ \mathcal{L}_{\text{rel-}\bar{\mathcal{R}}} &= - \frac{1}{2} \mu \bar{\mathcal{R}}_{\hat{0}\hat{k}\hat{\ell}} r^{\hat{k}} \dot{r}^{\hat{\ell}}. \end{aligned}$$

Here, $\mu = m_1 m_2 / (m_1 + m_2)$ is the reduced mass. When we consider only \mathcal{L}_{N} , we can separate the variables \mathbf{R} and \mathbf{r} . In particular, when the observer trajectory is a geodesic ($\mathbf{a} = 0$ and $\boldsymbol{\omega} = 0$), the orbit of $\mathbf{R} = 0$ becomes a solution of the equation for \mathbf{R} . This implies that the c.m. follows the observer's geodesic. Consequently, our analytical focus narrows down to the equation dictating the behavior of the relative coordinate \mathbf{r} . However, when we include the 0.5 PN term, it is not the case. The 0.5 PN Lagrangian $\mathcal{L}_{1/2}$ expression is written by use of \mathbf{R} and \mathbf{r} as follows:

$$\begin{aligned} \mathcal{L}_{1/2} &= \mathcal{L}_{1/2\text{-CM}}(\mathbf{R}, \dot{\mathbf{R}}) + \mathcal{L}_{1/2\text{-rel}}(\mathbf{r}, \dot{\mathbf{r}}) \\ &\quad + \mathcal{L}_{1/2\text{-int}}(\mathbf{R}, \dot{\mathbf{R}}, \mathbf{r}, \dot{\mathbf{r}}), \end{aligned} \quad (2.10)$$

where

$$\begin{aligned} \mathcal{L}_{1/2\text{-CM}}(\mathbf{R}, \dot{\mathbf{R}}) &= - \frac{2}{3} (m_1 + m_2) \bar{\mathcal{R}}_{\hat{0}\hat{k}\hat{j}\hat{\ell}} \mathbf{R}^{\hat{k}} \dot{\mathbf{R}}^{\hat{\ell}} \dot{\mathbf{R}}^{\hat{j}}, \\ \mathcal{L}_{1/2\text{-rel}}(\mathbf{r}, \dot{\mathbf{r}}) &= - \frac{2}{3} \mu \frac{(m_1 - m_2)}{(m_1 + m_2)} \bar{\mathcal{R}}_{\hat{0}\hat{k}\hat{j}\hat{\ell}} r^{\hat{k}} \dot{r}^{\hat{\ell}} \dot{r}^{\hat{j}}, \\ \mathcal{L}_{1/2\text{-int}}(\mathbf{R}, \dot{\mathbf{R}}, \mathbf{r}, \dot{\mathbf{r}}) &= - \frac{2}{3} \mu \bar{\mathcal{R}}_{\hat{0}\hat{k}\hat{j}\hat{\ell}} [r^{\hat{k}} \dot{r}^{\hat{\ell}} \dot{\mathbf{R}}^{\hat{j}} + (\mathbf{R}^{\hat{k}} \dot{r}^{\hat{\ell}} + r^{\hat{k}} \dot{\mathbf{R}}^{\hat{\ell}}) \dot{r}^{\hat{j}}]. \end{aligned} \quad (2.11)$$

The interaction term [Eq. (2.11)] invalidates the $\mathbf{R} = 0$ orbit as a solution, even when acceleration is absent. The coupling between the c.m. motion [$\mathbf{R}(\tau)$] and relative motion [$\mathbf{r}(\tau)$] makes both binary and c.m. trajectories intricate, even when the observer follows a geodesic. However, if we introduce an appropriate acceleration \mathbf{a} in 0.5 PN order to cancel the interaction terms, $\mathbf{R} = 0$ will become a solution, i.e., the c.m. can follow the observer's motion as follows: Integrating by parts the interaction term, we find

$$\begin{aligned} \mathcal{L}_{1/2\text{-int}}(\mathbf{R}, \dot{\mathbf{R}}, \mathbf{r}, \dot{\mathbf{r}}) &= - \frac{2}{3} \mu \bar{\mathcal{R}}_{\hat{0}\hat{k}\hat{j}\hat{\ell}} [\dot{\mathbf{R}}^{\hat{j}} r^{\hat{k}} \dot{r}^{\hat{\ell}} + \dot{r}^{\hat{j}} (\mathbf{R}^{\hat{k}} \dot{r}^{\hat{\ell}} + r^{\hat{k}} \dot{\mathbf{R}}^{\hat{\ell}})] \\ &\approx 2\mu \left[\frac{1}{3} \frac{d\bar{\mathcal{R}}_{\hat{0}\hat{k}\hat{j}\hat{\ell}}}{d\tau} r^{\hat{k}} \dot{r}^{\hat{\ell}} + \bar{\mathcal{R}}_{\hat{0}\hat{k}\hat{j}\hat{\ell}} r^{\hat{k}} \dot{r}^{\hat{\ell}} \right] \dot{\mathbf{R}}^{\hat{j}} \\ &\quad (\text{integration by part}), \end{aligned}$$

where the time derivative of the curvature is evaluated along the observer's orbit.

If we define the acceleration of the observer by

$$a_j = \frac{2\mu}{m_1 + m_2} \left[\frac{1}{3} \frac{d\bar{\mathcal{R}}_{\hat{0}\hat{k}\hat{j}\hat{\ell}}}{d\tau} r^{\hat{k}} r^{\hat{\ell}} + \bar{\mathcal{R}}_{\hat{0}\hat{k}\hat{j}\hat{\ell}} r^{\hat{k}} \dot{r}^{\hat{\ell}} \right],$$

two terms $\mathcal{L}_{1/2\text{-int}}$ and $\mathcal{L}_{\text{CM-}a}$ cancel each other. As a result, the Lagrangians for \mathbf{R} and \mathbf{r} are decoupled, and $\mathbf{R} = 0$ becomes an exact solution of the equation for \mathbf{R} , which is derived from the Lagrangian ($\mathcal{L}_{\text{CM}} + \mathcal{L}_{1/2\text{-CM}}$). The c.m. follows the observer's orbit and therefore, we obtain the decoupled equation for the relative coordinate \mathbf{r} .

To determine the proper observer's orbit, which deviates from a geodesic but remains in proximity to it, we must solve the equation of motion that accounts the small acceleration such that

$$\begin{aligned} \frac{Du_{\text{CM}}^\mu}{d\tau} &= a^\mu = e^{\mu\hat{j}} a_{\hat{j}} \\ &= \frac{2\mu}{m_1 + m_2} e^{\mu\hat{j}} \left[\frac{1}{3} \frac{d\bar{\mathcal{R}}_{\hat{0}\hat{k}\hat{j}\hat{\ell}}}{d\tau} r^{\hat{k}} r^{\hat{\ell}} + \bar{\mathcal{R}}_{\hat{0}\hat{k}\hat{j}\hat{\ell}} r^{\hat{k}} \dot{r}^{\hat{\ell}} \right]. \end{aligned} \quad (2.12)$$

This equation can also be expressed as

$$\begin{aligned} \frac{Dp_{\text{CM}}^\mu}{d\tau} &= (m_1 + m_2) a^\mu \\ &= e^{\mu\hat{j}} \left[\frac{1}{2} \bar{\mathcal{R}}_{\hat{0}\hat{j}\hat{k}\hat{\ell}} S^{\hat{k}\hat{\ell}} + \bar{\mathcal{R}}_{\hat{0}\hat{k}\hat{j}\hat{\ell}} \dot{M}^{\hat{k}\hat{\ell}} + \frac{2}{3} \frac{d\bar{\mathcal{R}}_{\hat{0}\hat{k}\hat{j}\hat{\ell}}}{d\tau} M^{\hat{k}\hat{\ell}} \right], \end{aligned} \quad (2.13)$$

where $p_{\text{CM}} \equiv (m_1 + m_2)u_{\text{CM}}$ is the c.m. 4-momentum, $S^{\hat{k}\hat{\ell}} \equiv r^{\hat{k}} p^{\hat{\ell}} - r^{\hat{\ell}} p^{\hat{k}}$ is the angular momentum tensor of a binary, and $M^{\hat{k}\hat{\ell}} \equiv \mu r^{\hat{k}} r^{\hat{\ell}}$ is the second mass moment, which can be replaced by the mass quadrupole moment $Q^{\hat{k}\hat{\ell}} \equiv r^{\hat{k}} r^{\hat{\ell}} - \frac{1}{3} r^2 \delta^{\hat{k}\hat{\ell}}$ in the Ricci-flat vacuum background. The first term in the right-hand side is the similar to the spin-curvature coupling term appeared in the Mathisson-Papapetrou-Dixon equations of a spinning test particle in a curved spacetime [64–66].

Consequently, our initial step involves solving the equation for the relative coordinate, denoted as \mathbf{r} , which is governed solely by the Lagrangian $\mathcal{L}_{\text{rel}}(\mathbf{r}) + \mathcal{L}_{1/2\text{-rel}}(\mathbf{r})$. Notably, when the masses are equal, i.e., $m_1 = m_2$, we have only the Newtonian Lagrangian \mathcal{L}_{rel} because $\mathcal{L}_{1/2\text{-rel}}$ vanishes. Once we have obtained the solution for $\mathbf{r}(\tau)$, we proceed to determine the motion of the c.m. or the observer within the background spacetime by addressing Eq. (2.12). Employing the solution for the relative motion $\mathbf{r}(\tau)$ in conjunction with the c.m. motion solution, represented as $x_{\text{CM}}^\mu(\tau)$, we can deduce the binary system's

trajectory within the specified curved background spacetime, denoted as $x_1^\mu(\tau)$ and $x_2^\mu(\tau)$.

III. EQUATION OF MOTION OF A BINARY SYSTEM IN A KERR SPACETIME

Now we consider a rotating SMBH as the background spacetime, which is given by Kerr solution in Boyer-Lindquist coordinates as

$$\begin{aligned} d\bar{s}^2 &= -\frac{\Delta}{\Sigma} (dt - a \sin^2 \theta d\phi)^2 + \frac{\sin^2 \theta}{\Sigma} [(r^2 + a^2) d\phi - a dt]^2 \\ &\quad + \frac{\Sigma}{\Delta} dr^2 + \Sigma d\theta^2, \end{aligned} \quad (3.1)$$

where

$$\Sigma = r^2 + a^2 \sin^2 \theta \quad \text{and} \quad \Delta = r^2 - 2Mr + a^2.$$

M and a are a gravitational mass and proper angular momentum of a supermassive black hole, respectively.

A. A test particle on the equatorial plane

We consider a circular geodesic on the equatorial plane of a test particle with a unit mass. The proper energy and proper angular momentum are determined by the radius \mathbf{r}_0 as

$$\mathfrak{E} = \frac{r_0^2 - 2Mr_0 + a\sigma\sqrt{Mr_0}}{r_0 F_\sigma(\mathbf{r}_0)}, \quad (3.2)$$

$$\mathfrak{L} = \frac{\sigma\sqrt{Mr_0}(r_0^2 + a^2 - 2a\sigma\sqrt{Mr_0})}{r_0 F_\sigma(\mathbf{r}_0)}, \quad (3.3)$$

where

$$F_\sigma(\mathbf{r}_0) \equiv \left(r_0^2 - 3Mr_0 + 2a\sigma\sqrt{Mr_0} \right)^{1/2},$$

and $\sigma = +1$ or -1 , which correspond to prograde and retrograde orbits, respectively. The existence condition of a circular orbit is

$$r_0^2 - 3Mr_0 + 2a\sigma\sqrt{Mr_0} \geq 0.$$

The innermost stable circular orbit (ISCO) is obtained by the conditions such that

$$\frac{d\mathfrak{E}}{dr_0} = 0, \quad \frac{d\mathfrak{L}}{dr_0} = 0,$$

which gives [67]

$$\frac{r_{\text{ISCO}}}{M} = 3 + Z_2 - \sigma[(3 - Z_1)(3 + Z_1 + 2Z_2)]^{1/2},$$

where

$$Z_1 = 1 + (1 - \chi^2)^{1/3} [(1 - \chi)^{1/3} + (1 + \chi)^{1/3}],$$

$$Z_2 = (3\chi^2 + Z_1^2)^{1/2},$$

with $\chi \equiv a/M$.

Since the energy and angular momentum are defined by

$$\mathfrak{E} = -u_t, \quad \mathfrak{L} = u_\phi,$$

we find

$$u^t = \frac{\mathbf{r}_0^2 + a\sigma\sqrt{M\mathbf{r}_0}}{\mathbf{r}_0 F_\sigma(\mathbf{r}_0)},$$

$$u^\phi = \frac{\sigma\sqrt{M\mathbf{r}_0}}{\mathbf{r}_0 F_\sigma(\mathbf{r}_0)}.$$

From the latter equation, we find the angular velocity of a circular observer measured by the proper time as

$$\frac{d\phi}{d\tau} = u^\phi = \sigma\mathfrak{w}_0,$$

where

$$\mathfrak{w}_0 \equiv \frac{\sqrt{M\mathbf{r}_0}}{\mathbf{r}_0 F_\sigma(\mathbf{r}_0)}.$$

B. A local inertial reference frame

For the present purpose, there is one convenient tetrad system of Kerr spacetime, which is called Carter's tetrad system such that

$$e^\mu_{\bar{t}} = \frac{1}{\sqrt{\Sigma\Delta}}(r^2 + a^2, 0, 0, a),$$

$$e^\mu_{\bar{r}} = \sqrt{\frac{\Delta}{\Sigma}}(0, 1, 0, 0),$$

$$e^\mu_{\bar{\theta}} = \frac{1}{\sqrt{\Sigma}}(0, 0, 1, 0),$$

$$e^\mu_{\bar{\phi}} = \frac{1}{\sqrt{\Sigma}}\left(a \sin\theta, 0, 0, \frac{1}{\sin\theta}\right).$$

Now we construct a local inertial reference frame along the observer. The transformation matrix from Carter's tetrad to a rotating proper reference frame (τ, x, y, z) is given by

$$\Lambda_{\bar{0}}^{\bar{\alpha}} = \left(\frac{\mathfrak{E}(\mathbf{r}_0^2 + a^2) - a\mathfrak{L}}{\mathbf{r}_0\sqrt{\Delta}}, 0, 0, \frac{\mathfrak{L} - a\mathfrak{E}}{\mathbf{r}_0}\right),$$

$$\Lambda_{\bar{x}}^{\bar{\alpha}} = \frac{1}{\sqrt{S}}(0, \mathbf{r}_0\Lambda_{\bar{0}}^{\bar{0}}, 0, 0),$$

$$\Lambda_{\bar{y}}^{\bar{\alpha}} = \sigma\sqrt{\frac{K}{S}}\left(\Lambda_{\bar{0}}^{\bar{0}}, 0, 0, \frac{S}{K}\Lambda_{\bar{0}}^{\bar{\phi}}\right),$$

$$\Lambda_{\bar{z}}^{\bar{\alpha}} = \frac{\sigma}{\sqrt{K}}(0, 0, -\mathbf{r}_0\Lambda_{\bar{0}}^{\bar{\phi}}, 0),$$

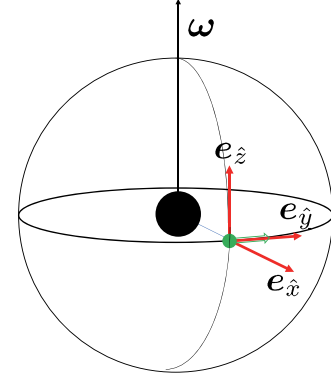


FIG. 1. A tetrad system $\{e_{\bar{x}}, e_{\bar{y}}, e_{\bar{z}}\}$ rotating with an angular velocity \mathfrak{w}_0 along a circular orbit.

where

$$K \equiv (\mathfrak{L} - a\mathfrak{E})^2,$$

$$S \equiv \mathbf{r}_0^2 + K.$$

K is the so-called Carter's constant.

Here, we choose the Descartes coordinates (x, y, z) as shown in Fig. 1.

Inserting Eqs. (3.2) and (3.3), we obtain the transformation matrix $\Lambda_{\bar{\alpha}}^{\bar{\lambda}}$ as

$$\Lambda_{\bar{0}}^{\bar{\lambda}} = \frac{1}{F_\sigma(\mathbf{r}_0)}(\sqrt{\Delta(\mathbf{r}_0)}, 0, 0, \sigma\sqrt{M\mathbf{r}_0} - a), \quad (3.4)$$

$$\Lambda_{\bar{x}}^{\bar{\lambda}} = (0, 1, 0, 0), \quad (3.5)$$

$$\Lambda_{\bar{y}}^{\bar{\lambda}} = \frac{1}{F_\sigma(\mathbf{r}_0)}(\sigma\sqrt{M\mathbf{r}_0} - a, 0, 0, \sqrt{\Delta(\mathbf{r}_0)}), \quad (3.6)$$

$$\Lambda_{\bar{z}}^{\bar{\lambda}} = (0, 0, -1, 0), \quad (3.7)$$

which provides the tetrad of the rotating proper reference frame $e_{\bar{\alpha}}^\mu \equiv \Lambda_{\bar{\alpha}}^{\bar{\lambda}} e_{\bar{\lambda}}^\mu$ as

$$e_{\bar{0}}^\mu \equiv \frac{1}{\mathbf{r}_0 F_\sigma(\mathbf{r}_0)}(\mathbf{r}_0^2 + a\sigma\sqrt{M\mathbf{r}_0}, 0, 0, \sigma\sqrt{M\mathbf{r}_0}),$$

$$e_{\bar{x}}^\mu = \left(0, \frac{\sqrt{\Delta(\mathbf{r}_0)}}{\mathbf{r}_0}, 0, 0\right),$$

$$e_{\bar{y}}^\mu = \frac{1}{\mathbf{r}_0 F_\sigma(\mathbf{r}_0) \sqrt{\Delta(\mathbf{r}_0)}}\left(\sigma\sqrt{M\mathbf{r}_0}[\mathbf{r}_0^2 + a^2 - 2a\sigma\sqrt{M\mathbf{r}_0}], 0, 0, \mathbf{r}_0^2 - 2M\mathbf{r}_0 + a\sigma\sqrt{M\mathbf{r}_0}\right),$$

$$e_{\bar{z}}^\mu = \left(0, 0, -\frac{1}{\mathbf{r}_0}, 0\right).$$

To discuss the dynamics of a binary, nonrotating proper reference frame is more convenient. We then rotate the xy -plane as $((x, y) \rightarrow (\mathbf{x}, \mathbf{y}))$, with transformation given by

$$\begin{aligned}\tilde{\Lambda}_x^{\bar{\alpha}} &= \Lambda_x^{\bar{\alpha}} \cos \Psi(\tau) - \Lambda_y^{\bar{\alpha}} \sin \Psi(\tau), \\ \tilde{\Lambda}_y^{\bar{\alpha}} &= \Lambda_x^{\bar{\alpha}} \sin \Psi(\tau) + \Lambda_y^{\bar{\alpha}} \cos \Psi(\tau),\end{aligned}$$

where the rotation angle Ψ satisfies the evolution equation such that

$$\dot{\Psi} = \sigma \frac{\sqrt{K}}{r_0^2} \left(\frac{\mathcal{G}(r_0^2 + a^2) - a\mathcal{L}}{S} + \frac{a(\mathcal{L} - a\mathcal{G})}{K} \right) = \sigma \mathfrak{w}_R,$$

with

$$\mathfrak{w}_R = \frac{M^{1/2}}{r_0^{3/2}},$$

being the angular frequency of the rotating frame. It gives

$$\Psi = \sigma \mathfrak{w}_R \tau.$$

In order to revert to the nonrotating frame, we have to transform back using the angular velocity. The difference between the two angular velocities

$$\mathfrak{w}_P \equiv \mathfrak{w}_0 - \mathfrak{w}_R,$$

gives rotation of inertial frame. It also gives the precession of the angular momentum as we will show it later. It contains two relativistic precessions, i.e., the so-called de-Sitter precession and the Lense-Thirring precession. This is evident when we take the limit of $M/r_0 \ll 1$. Since $a \leq M$, this limit gives $a/r_0 \ll 1$. In this limit, we find

$$\begin{aligned}\mathfrak{w}_0 &= \frac{\sqrt{M r_0}}{r_0(r_0^2 - 3M r_0 + 2a\sigma\sqrt{M r_0})^{1/2}} \\ &\approx \frac{M^{1/2}}{r_0^{3/2}} \left[1 + \frac{3M}{2r_0} - \frac{a\sigma}{r_0} \sqrt{\frac{M}{r_0}} \right] \\ &= \mathfrak{w}_R + \mathfrak{w}_{\text{dS}} + \mathfrak{w}_{\text{LT}},\end{aligned}$$

where

$$\begin{aligned}\mathfrak{w}_{\text{dS}} &= \frac{3M}{2r_0} \mathfrak{w}_R = \frac{3M^{3/2}}{2r_0^{5/2}}, \\ \mathfrak{w}_{\text{LT}} &= -\frac{a\sigma}{r_0} \sqrt{\frac{M}{r_0}} \mathfrak{w}_R = -\frac{Ma\sigma}{r_0^3}.\end{aligned}$$

The frequencies \mathfrak{w}_{dS} and \mathfrak{w}_{LT} correspond to those of de-Sitter and Lense-Thirring precessions, respectively.

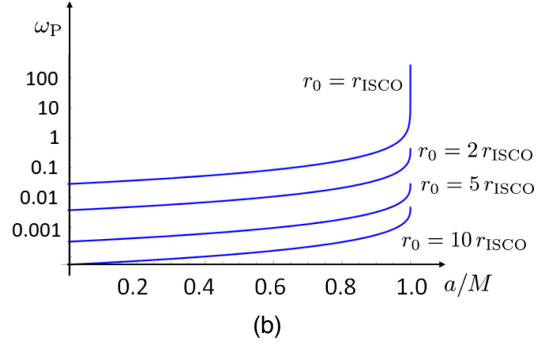
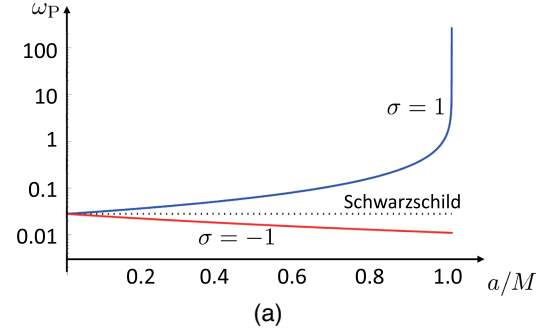


FIG. 2. The precession frequency \mathfrak{w}_P in terms of the Kerr parameter a/M . (a) The position of the c.m. \mathbf{r}_0 is chosen at the ISCO radius. (b) \mathbf{r}_0 for prograde orbits are chosen as $\mathbf{r}_0 = \mathbf{r}_{\text{ISCO}}, 2\mathbf{r}_{\text{ISCO}}, 5\mathbf{r}_{\text{ISCO}},$ and $10\mathbf{r}_{\text{ISCO}}$.

These two frequencies are quite similar to those discussed in [35,36].

In Fig. 2, we show the behavior of \mathfrak{w}_P in terms of the Kerr parameter a . In Fig. 2(a), we set $\mathbf{r}_0 = \mathbf{r}_{\text{ISCO}}$, and in Fig. 2(b), we change the radius as $\mathbf{r}_0/\mathbf{r}_{\text{ISCO}} = 1, 2, 5,$ and 10 .

We find that \mathfrak{w}_P gets larger as a increases and this increase become particularly rapid near the extreme limit of $a \rightarrow 1$, which means that the Lense-Thirring precession becomes dominant. The critical value a_{cr} , beyond which the Lense-Thirring precession is larger than the de-Sitter precession, is evaluated by

$$\mathfrak{w}_P(a_{\text{cr}}) = 2\mathfrak{w}_{\text{dS}},$$

where $\mathfrak{w}_{\text{dS}} = \mathfrak{w}_P(a = 0)$. In the case of $\mathbf{r}_0 = \mathbf{r}_{\text{ISCO}}$, we find $a_{\text{cr}} \approx 0.43185973M$.

However when we fix the radius \mathbf{r}_0 , \mathfrak{w}_P does not depend on a so much as shown in Fig. 3. We show the cases of $\mathbf{r}_0 = 6M$ and $\mathbf{r}_0 = 10M$. For $\mathbf{r}_0 = 6M$, we give only for the prograde orbits because the ISCO radius for the retrograde orbits is larger than $6M$.

In the prograde orbits, it decreases as a increases, while it increases for the retrograde orbits.

C. Riemann curvature components in rotating proper reference frame

The nontrivial components of the Riemann curvature in the Carter's tetrad system are given by

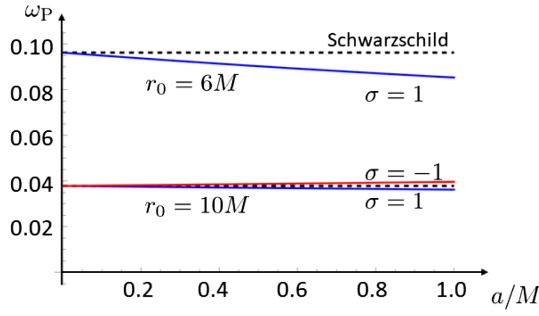


FIG. 3. The precession frequency ω_P in terms of a . We fix the position of the c.m. at $\mathbf{r}_0 = 10M$ and $6M$. The blue and red curves denote the prograde and retrograde cases, respectively. The value for $a = 0$ is also given by the black dashed lines as reference.

$$\begin{aligned} R_{\bar{i}\bar{\phi}\bar{i}\bar{\phi}} &= -R_{\bar{i}\bar{\theta}\bar{i}\bar{\theta}} = -\frac{1}{2}R_{\bar{i}\bar{\tau}\bar{i}\bar{\tau}} = \frac{1}{2}R_{\bar{\theta}\bar{\phi}\bar{\theta}\bar{\phi}} \\ &= R_{\bar{i}\bar{\theta}\bar{i}\bar{\theta}} = -R_{\bar{i}\bar{\tau}\bar{i}\bar{\tau}} = Q_1, \\ R_{\bar{i}\bar{\phi}\bar{i}\bar{\theta}} &= \frac{1}{2}R_{\bar{i}\bar{\tau}\bar{i}\bar{\phi}} = R_{\bar{i}\bar{\theta}\bar{i}\bar{\tau}} = -Q_2, \end{aligned}$$

where

$$\begin{aligned} Q_1 &= \frac{M\mathbf{r}(\mathbf{r}^2 - 3a^2\cos^2\theta)}{\Sigma^3} \\ Q_2 &= \frac{Ma\cos\theta(3\mathbf{r}^2 - a^2\cos^2\theta)}{\Sigma^3}. \end{aligned}$$

On the equatorial plane ($\theta = \pi/2$), we find simpler expression such that the nontrivial components are very similar to the Schwarzschild case as

$$\begin{aligned} R_{\bar{i}\bar{\theta}\bar{i}\bar{\theta}} &= R_{\bar{i}\bar{\phi}\bar{i}\bar{\phi}} = -R_{\bar{i}\bar{\tau}\bar{i}\bar{\tau}} = -R_{\bar{i}\bar{\phi}\bar{i}\bar{\tau}} = \frac{M}{\mathbf{r}^3} \\ R_{\bar{\theta}\bar{\phi}\bar{\theta}\bar{\phi}} &= -R_{\bar{i}\bar{\tau}\bar{i}\bar{\tau}} = \frac{2M}{\mathbf{r}^3}. \end{aligned} \quad (3.8)$$

Since we know the Riemann curvature components in the Carter's tetrad frame [Eq. (3.8)] and the transformation matrix $\Lambda_{\bar{\alpha}}^{\bar{\lambda}}$ to the rotating proper reference frame [Eqs. (3.4)–(3.7)], we can easily find the nontrivial Riemann curvature components in rotating proper reference frame as

$$\begin{aligned} \bar{\mathcal{R}}_{\hat{0}\hat{x}\hat{0}\hat{x}} &= -\bar{\mathcal{R}}_{\hat{y}\hat{z}\hat{y}\hat{z}} \\ &= -\frac{M}{F_{\sigma}^2(\mathbf{r}_0)\mathbf{r}_0^3}(2\mathbf{r}_0^2 + 3a^2 - 3M\mathbf{r}_0 - 2a\sigma\sqrt{M\mathbf{r}_0}), \\ \bar{\mathcal{R}}_{\hat{0}\hat{y}\hat{0}\hat{y}} &= -\bar{\mathcal{R}}_{\hat{z}\hat{x}\hat{z}\hat{x}} = \frac{M}{\mathbf{r}_0^3}, \\ \bar{\mathcal{R}}_{\hat{0}\hat{z}\hat{0}\hat{z}} &= -\bar{\mathcal{R}}_{\hat{x}\hat{y}\hat{x}\hat{y}} = \frac{M}{F_{\sigma}^2(\mathbf{r}_0)\mathbf{r}_0^3}(\mathbf{r}_0^2 + 3a^2 - 4a\sigma\sqrt{M\mathbf{r}_0}), \\ \bar{\mathcal{R}}_{\hat{0}\hat{x}\hat{y}\hat{x}} &= -\bar{\mathcal{R}}_{\hat{0}\hat{z}\hat{y}\hat{z}} = -\frac{3M}{F_{\sigma}^2(\mathbf{r}_0)\mathbf{r}_0^3}\sqrt{\Delta(\mathbf{r}_0)}(\sigma\sqrt{M\mathbf{r}_0} - a). \end{aligned}$$

D. Equations of motion of a binary

Since the c.m. of a binary follows the observer's circular geodesic ($\mathbf{R} = 0$), we have to solve only the equations of motion for the relative coordinate \mathbf{r} . Using $x = r^{\hat{1}}$, $y = r^{\hat{2}}$, $z = r^{\hat{3}}$, the relative motion of a binary is given by the Lagrangian

$$\begin{aligned} \mathcal{L}_{\text{rel}}(\mathbf{r}, \dot{\mathbf{r}}) &= \frac{1}{2}\mu\dot{\mathbf{r}}^2 + \frac{Gm_1m_2}{r} + \mathcal{L}_{\text{rel-}\mathfrak{w}}(\mathbf{r}, \dot{\mathbf{r}}) \\ &\quad + \mathcal{L}_{\text{rel-}\bar{\mathcal{R}}}(\mathbf{r}, \dot{\mathbf{r}}), \end{aligned} \quad (3.9)$$

with

$$\begin{aligned} \mathcal{L}_{\text{rel-}\mathfrak{w}} &= -\mu \left[\sigma\mathfrak{w}_0(xy - yx) - \frac{\mathfrak{w}_0^2}{2}(x^2 + y^2) \right], \\ \mathcal{L}_{\text{rel-}\bar{\mathcal{R}}} &= -\frac{\mu}{2}(\bar{\mathcal{R}}_{\hat{0}\hat{x}\hat{0}\hat{x}}x^2 + \bar{\mathcal{R}}_{\hat{0}\hat{y}\hat{0}\hat{y}}y^2 + \bar{\mathcal{R}}_{\hat{0}\hat{z}\hat{0}\hat{z}}z^2) \\ &= -\frac{\mu M}{2\mathbf{r}_0^3} \left[r^2 + \frac{3}{F_{\sigma}^2(\mathbf{r}_0)}(-\Delta(\mathbf{r}_0)x^2 + (\sigma\sqrt{M\mathbf{r}_0} - a)z^2) \right]. \end{aligned}$$

The first and second terms in $\mathcal{L}_{\text{rel-}\mathfrak{w}}$ describe the Coriolis force and the centrifugal force, respectively. The first half terms in $\mathcal{L}_{\text{rel-}\bar{\mathcal{R}}}$ are the same as those in Newtonian hierarchical triple system under quadrupole approximation. Note that in the present approach (approximation up to the second order of $r^{\hat{i}}$), we cannot go beyond quadrupole approximation.

In order to analyze the relative motion of a binary, it is better to work in a nonrotating initial reference frame. Since the angular frequency of a rotating tetrad frame is $\mathfrak{w}_{\mathbf{R}}$, the position (x, y, z) in the rotating frame can be replaced by the position $(\mathbf{x}, \mathbf{y}, \mathbf{z})$ in a nonrotating Descartes coordinate system by use of the following transformation;

$$\begin{aligned} x &= \mathbf{x} \cos \sigma\mathfrak{w}_{\mathbf{R}}\tau - \mathbf{y} \sin \sigma\mathfrak{w}_{\mathbf{R}}\tau, \\ y &= \mathbf{x} \sin \sigma\mathfrak{w}_{\mathbf{R}}\tau + \mathbf{y} \cos \sigma\mathfrak{w}_{\mathbf{R}}\tau, \\ z &= \mathbf{z}. \end{aligned}$$

The Lagrangian \mathcal{L}_{rel} in a nonrotating proper reference frame is given by

$$\begin{aligned} \mathcal{L}_{\text{rel}} &= \frac{1}{2}\mu \left(\frac{d\mathbf{r}}{d\tau} \right)^2 + \frac{Gm_1m_2}{r} + \mathcal{L}_{\text{rel-P}}(\mathbf{r}, \dot{\mathbf{r}}) \\ &\quad + \mathcal{L}_{\text{rel-}\bar{\mathcal{R}}}(\mathbf{r}, \tau), \end{aligned} \quad (3.10)$$

where

$$\mathcal{L}_{\text{rel-P}}(\mathbf{r}, \dot{\mathbf{r}}) = \mu \sigma \mathfrak{w}_P (\dot{x}y - \dot{y}x) + \frac{\mu}{2} \mathfrak{w}_P^2 (x^2 + y^2),$$

$$\mathcal{L}_{\text{rel-}\bar{\mathcal{R}}}(\mathbf{r}, \tau) = -\frac{\mu M}{2\mathbf{r}_0^3} \left[r^2 + \frac{3}{F_\sigma^2(\mathbf{r}_0)} (-\Delta(\mathbf{r}_0)(x \cos \sigma \mathfrak{w}_R \tau - y \sin \sigma \mathfrak{w}_R \tau)^2 + (\sigma \sqrt{M \mathbf{r}_0} - a)^2 z^2) \right].$$

Since the momentum is defined by

$$\begin{aligned} p_x &\equiv \frac{\partial \mathcal{L}}{\partial \dot{x}} = \mu \dot{x} + \mu \sigma \mathfrak{w}_P y, \\ p_y &\equiv \frac{\partial \mathcal{L}}{\partial \dot{y}} = \mu \dot{y} - \mu \sigma \mathfrak{w}_P x, \\ p_z &\equiv \frac{\partial \mathcal{L}}{\partial \dot{z}} = \mu \dot{z}, \end{aligned}$$

we obtain the Hamiltonian as

$$\mathcal{H}_{\text{rel}} = \mathcal{H}_0 + \mathcal{H}_1, \quad (3.11)$$

where

$$\begin{aligned} \mathcal{H}_0 &= \frac{1}{2\mu} \mathbf{p}^2 - \frac{Gm_1 m_2}{r}, \\ \mathcal{H}_1 &= \mathcal{H}_{1-P} + \mathcal{H}_{1-\bar{\mathcal{R}}}, \end{aligned}$$

with

$$\begin{aligned} \mathcal{H}_{1-P} &= \sigma \mathfrak{w}_P (p_y x - p_x y), \\ \mathcal{H}_{1-\bar{\mathcal{R}}} &= \frac{\mu M}{2\mathbf{r}_0^3} \left[r^2 + \frac{3}{F_\sigma^2(\mathbf{r}_0)} (-\Delta(\mathbf{r}_0)(x \cos \sigma \mathfrak{w}_R \tau - y \sin \sigma \mathfrak{w}_R \tau)^2 + (\sigma \sqrt{M \mathbf{r}_0} - a)^2 z^2) \right]. \end{aligned}$$

The equations of motion are given as

$$\dot{x} = \frac{\partial \mathcal{H}}{\partial p_x} = \frac{p_x}{\mu} - \sigma \mathfrak{w}_P y, \quad (3.12)$$

$$\dot{y} = \frac{\partial \mathcal{H}}{\partial p_y} = \frac{p_y}{\mu} + \sigma \mathfrak{w}_P x, \quad (3.13)$$

$$\dot{z} = \frac{\partial \mathcal{H}}{\partial p_z} = \frac{p_z}{\mu}, \quad (3.14)$$

and

$$\begin{aligned} \dot{p}_x &= -\frac{\partial \mathcal{H}}{\partial x} = -\frac{Gm_1 m_2}{r^3} x - \sigma \mathfrak{w}_P p_y \\ &\quad - \frac{\mu M}{\mathbf{r}_0^3} [x - 3\lambda(x \cos \sigma \mathfrak{w}_R \tau - y \sin \sigma \mathfrak{w}_R \tau) \cos \mathfrak{w}_R \tau], \end{aligned} \quad (3.15)$$

$$\begin{aligned} \dot{p}_y &= -\frac{\partial \mathcal{H}}{\partial y} = -\frac{Gm_1 m_2}{r^3} y + \sigma \mathfrak{w}_P p_x \\ &\quad - \frac{\mu M}{\mathbf{r}_0^3} [y + 3\lambda(x \cos \sigma \mathfrak{w}_R \tau - y \sin \sigma \mathfrak{w}_R \tau) \sin \mathfrak{w}_R \tau], \end{aligned} \quad (3.16)$$

$$\dot{p}_z = -\frac{\partial \mathcal{H}}{\partial z} = -\frac{Gm_1 m_2}{r^3} z - \frac{\mu M}{\mathbf{r}_0^3} [-2 + 3\lambda] z, \quad (3.17)$$

where

$$\lambda \equiv \frac{\Delta(\mathbf{r}_0)}{F_\sigma^2(\mathbf{r}_0)} = \frac{\mathbf{r}_0^2 - 2M\mathbf{r}_0 + a^2}{\mathbf{r}_0^2 - 3M\mathbf{r}_0 + 2a\sigma\sqrt{M\mathbf{r}_0}}. \quad (3.18)$$

IV. PRELIMINARY CONSIDERATIONS

For numerical analysis in next section, we shall first rewrite the basic equations using dimensionless variables, introduce the orbital parameters, show how to set up initial data, and discuss validity of the present model and stability condition.

A. Normalization

In this paper we will analyze a binary model with $m_1 = m_2$. We have to solve Eqs. (3.12)–(3.17). In order to solve these basic equations, we shall introduce dimensionless variables as follows: Since we consider a hierarchical triple system, the initial motion of a binary can be approximated by an elliptic orbit. Hence, the length scale of a binary is normalized by an initial semimajor axis \mathbf{a}_0 , while timescale is normalized by an initial binary mean motion n_0 , which is defined by

$$n_0 \equiv \left(\frac{G(m_1 + m_2)}{\mathbf{a}_0^3} \right)^{1/2}.$$

Note that the initial binary period is given by $P_{\text{in}} = 2\pi/n_0$.

Introducing

$$\begin{aligned}\tilde{\tau} &= n_0\tau, \\ \tilde{\mathbf{x}} &= \frac{\mathbf{x}}{\mathbf{a}_0}, \tilde{\mathbf{y}} = \frac{\mathbf{y}}{\mathbf{a}_0}, \tilde{\mathbf{z}} = \frac{\mathbf{z}}{\mathbf{a}_0}, \tilde{\mathbf{r}} = \frac{\mathbf{r}}{\mathbf{a}_0}, \\ \tilde{\rho}_x &= \frac{\rho_x}{\mu\mathbf{a}_0n_0}, \tilde{\rho}_y = \frac{\rho_y}{\mu\mathbf{a}_0n_0}, \tilde{\rho}_z = \frac{\rho_z}{\mu\mathbf{a}_0n_0},\end{aligned}$$

we find

$$\frac{d\tilde{\mathbf{x}}}{d\tilde{\tau}} = \tilde{\rho}_x - \sigma\tilde{\mathbf{w}}_P\tilde{\mathbf{y}}, \quad (4.1)$$

$$\frac{d\tilde{\mathbf{y}}}{d\tilde{\tau}} = \tilde{\rho}_y + \sigma\tilde{\mathbf{w}}_P\tilde{\mathbf{x}}, \quad (4.2)$$

$$\frac{d\tilde{\mathbf{z}}}{d\tilde{\tau}} = \tilde{\rho}_z, \quad (4.3)$$

and

$$\begin{aligned}\frac{d\tilde{\rho}_x}{d\tilde{\tau}} &= -\frac{\tilde{\mathbf{x}}}{\tilde{r}^3} - \sigma\tilde{\mathbf{w}}_P\tilde{\rho}_y \\ &\quad - \frac{1}{\tilde{f}}[\tilde{\mathbf{x}} - 3\lambda(\tilde{\mathbf{x}}\cos\sigma\tilde{\mathbf{w}}_R\tilde{\tau} - \tilde{\mathbf{y}}\sin\sigma\tilde{\mathbf{w}}_R\tilde{\tau})\cos\sigma\tilde{\mathbf{w}}_R\tilde{\tau}],\end{aligned} \quad (4.4)$$

$$\begin{aligned}\frac{d\tilde{\rho}_y}{d\tilde{\tau}} &= -\frac{\tilde{\mathbf{y}}}{\tilde{r}^3} + \sigma\tilde{\mathbf{w}}_P\tilde{\rho}_x \\ &\quad - \frac{1}{\tilde{f}}[\tilde{\mathbf{y}} + 3\lambda(\tilde{\mathbf{x}}\cos\sigma\tilde{\mathbf{w}}_R\tilde{\tau} - \tilde{\mathbf{y}}\sin\sigma\tilde{\mathbf{w}}_R\tilde{\tau})\sin\sigma\tilde{\mathbf{w}}_R\tilde{\tau}],\end{aligned} \quad (4.5)$$

$$\frac{d\tilde{\rho}_z}{d\tilde{\tau}} = -\frac{\tilde{\mathbf{z}}}{\tilde{r}^3} - \frac{1}{\tilde{f}}(-2 + 3\lambda)\tilde{\mathbf{z}}, \quad (4.6)$$

where

$$\begin{aligned}\tilde{\mathbf{w}}_P &\equiv \frac{\mathbf{w}_P}{n_0}, \\ \tilde{\mathbf{w}}_R &\equiv \frac{\mathbf{w}_R}{n_0},\end{aligned}$$

and

$$\lambda = \frac{\mathbf{r}_0^2 - 2M\mathbf{r}_0 + a^2}{\mathbf{r}_0^2 - 3M\mathbf{r}_0 + 2a\sigma\sqrt{M}\mathbf{r}_0}.$$

\tilde{f} denotes the firmness parameter of a binary, which is defined by

$$\begin{aligned}\tilde{f} &\equiv \frac{\text{gravitational force}}{\text{tidal force by SMBH}} = \frac{Gm_1m_2/\mathbf{a}_0^2}{G\mu M\mathbf{a}_0/\mathbf{r}_0^3} \\ &= \left(\frac{m_1 + m_2}{M}\right)\left(\frac{\mathbf{r}_0}{\mathbf{a}_0}\right)^3.\end{aligned}$$

The initial semimajor axis \mathbf{a}_0 is given by

$$\mathbf{a}_0 = \tilde{f}^{-\frac{1}{3}}\left(\frac{m_1 + m_2}{M}\right)^{1/3}\mathbf{r}_0. \quad (4.7)$$

Using \tilde{f} , we find

$$\tilde{\mathbf{w}}_P = \nu\tilde{f}^{-\frac{1}{2}}, \quad (4.8)$$

$$\tilde{\mathbf{w}}_R = \tilde{f}^{-\frac{1}{2}}, \quad (4.9)$$

where

$$\nu \equiv \frac{\mathbf{r}_0}{F_\sigma(\mathbf{r}_0)} - 1 = \frac{\mathbf{r}_0}{\sqrt{\mathbf{r}_0^2 - 3M\mathbf{r}_0 + 2a\sigma\sqrt{M}\mathbf{r}_0}} - 1. \quad (4.10)$$

The basic equations (4.1)–(4.6) contain three independent parameters; λ , ν , and the firmness \tilde{f} . λ changes from 1 to 4/3, while ν runs from 0 to $\sqrt{2} - 1$ for $a = 0$ and to ∞ for $a = M$.

As for the firmness \tilde{f} , as we will discuss it later, $\tilde{f} \gg 1$ is required for stability. In the limit of $\tilde{f} \rightarrow \infty$, we find an integrable system. The orbit shows the precession with the period $\tilde{\mathbf{w}}_P$.

B. Orbital parameters

In order to discuss the properties of a binary orbit, it is more convenient to use the orbital parameters. We may assume that the binary motion is close to an elliptic orbit, which is described by

$$\mathbf{r} = \frac{\mathbf{a}(1 - e^2)}{1 + e\cos f},$$

where \mathbf{a} is a semimajor axis, e is the eccentricity, and f is true anomaly. Since the orbital plane is not, in general, $\mathbf{z} = 0$, we have to introduce three angular variables; the argument of periapsis ω , the ascending node Ω and the inclination angle I . We have the relations between the position $\mathbf{r} = (x, y, z)$ of the component of a binary and the orbital parameters $(\omega, \Omega, \mathbf{a}, e, I, f)$ as

$$\begin{pmatrix} x \\ y \\ z \end{pmatrix} = r \begin{pmatrix} \cos\Omega\cos(\omega + f) - \sin\Omega\sin(\omega + f)\cos I \\ \sin\Omega\cos(\omega + f) + \cos\Omega\sin(\omega + f)\cos I \\ \sin(\omega + f)\sin I \end{pmatrix}. \quad (4.11)$$

In order to extract the orbital parameters from the orbit given by the Cartesian coordinates, one can use the

osculating orbit when the orbit is close to an ellipse. The magnitude of the normalized Laplace-Runge-Lenz vector, which is defined by

$$\mathbf{e} \equiv \tilde{\mathbf{p}} \times (\tilde{\mathbf{r}} \times \tilde{\mathbf{p}}) - \frac{\tilde{\mathbf{r}}}{\tilde{r}}, \quad (4.12)$$

is commonly used for a measure of orbital eccentricity.

The inclination angle I is defined as mutual inclination between angular momenta of the inner and outer binary.

$$I = \cos^{-1} \left(\frac{\tilde{L}_z}{|\tilde{\mathbf{L}}|} \right), \quad (4.13)$$

where $\tilde{\mathbf{L}} \equiv \tilde{\mathbf{r}} \times \tilde{\mathbf{p}}$ is the angular momentum of a binary.

The other two essential angles Ω and ω governing the orientation of the orbital plane. The line that marks the intersection of the orbital plane with the reference plane (the equatorial plane in the present case) is called the node line, and the point on the node line where the orbit passes above the reference plane from below is called the ascending node. The angle between the reference axis (say x-axis) and node line vector \mathbf{N} is the longitude of ascending node Ω . First, node line is defined as

$$\mathbf{N} = \hat{\mathbf{z}} \times \tilde{\mathbf{L}}. \quad (4.14)$$

where $\hat{\mathbf{z}}$ is normal to the reference plane (the unit vector in the z direction). Thus, Ω is computed as

$$\Omega = \cos^{-1}(N_x/N). \quad (4.15)$$

The argument of periaapsis ω is the angle between node line and periaapsis measured in the direction of motion. Therefore,

$$\omega = \cos^{-1} \left(\frac{\mathbf{N} \cdot \mathbf{e}}{N e} \right). \quad (4.16)$$

However, one must be careful with the definitions of orbital elements when using the osculating method. Notably, eccentricity can exhibit unusual behavior, such as ‘‘apparent’’ rise or unphysical rapid oscillations, particularly when dealing with very small eccentricities and using the magnitude of the Runge-Lenz vector as an eccentricity measure, as observed in [68]. In such a case, it is better to define the eccentricity by the averaged one over one cycle as

$$\langle e \rangle \equiv \frac{r_{\max} - r_{\min}}{r_{\max} + r_{\min}},$$

where r_{\max} and r_{\min} correspond to orbital separation at adjacent turning points of an eccentric orbit.

When the orbit can be approximated well by the osculating one, \mathbf{e} is given by the normalized Laplace-Runge-Lenz

vector (4.12). Otherwise, we define the averaged eccentricity vector by

$$\langle \mathbf{e} \rangle \equiv - \frac{(\mathbf{r}_{\min} + \mathbf{r}_{\max})}{(r_{\min} + r_{\max})}$$

pointing towards the periaapsis, where \mathbf{r}_{\max} and \mathbf{r}_{\min} are obtained from the numerical data of position vectors. We have used both definitions and found that most results agree well.

C. Initial data

In order to provide the initial data of a binary, i.e., $\tilde{\mathbf{x}}_0, \tilde{\mathbf{y}}_0, \tilde{\mathbf{z}}_0$ and $\tilde{\mathbf{p}}_{x0}, \tilde{\mathbf{p}}_{y0}, \tilde{\mathbf{p}}_{z0}$, we shall give the initial orbital parameters $(\omega_0, \Omega_0, \alpha_0, e_0)$. From (4.11), assuming $f = 0$ at $\tau = 0$, we find

$$\begin{aligned} \tilde{\mathbf{x}}_0 &= (1 - e_0)[\cos \Omega_0 \cos \omega_0 - \sin \Omega_0 \sin \omega_0 \cos I_0], \\ \tilde{\mathbf{y}}_0 &= (1 - e_0)[\sin \Omega_0 \cos \omega_0 + \cos \Omega_0 \sin \omega_0 \cos I_0], \\ \tilde{\mathbf{z}}_0 &= (1 - e_0) \sin \omega_0 \sin I_0. \end{aligned}$$

As for the momentum $\tilde{\mathbf{p}}_{x0}, \tilde{\mathbf{p}}_{y0}, \tilde{\mathbf{p}}_{z0}$, we use the definitions of the orbital parameters of the osculating orbit, i.e., Eqs. (4.12), (4.13), (4.16), and (4.15) with (4.14).

From Eq. (4.14) we find

$$N_{x0} = -\tilde{L}_{y0}, \quad N_{y0} = \tilde{L}_{x0}, \quad N_{z0} = 0.$$

From Eq. (4.15) we obtain

$$N_{x0} = N_0 \cos \Omega_0.$$

Since $N_0^2 = N_{x0}^2 + N_{y0}^2$, we find

$$N_{y0} = N_0 \sin \Omega_0.$$

Hence, from Eq. (4.16), we find

$$e_0 \cos \omega_0 = \left(\frac{N_0}{N_0} \cdot \mathbf{e}_0 \right) = \cos \Omega_0 e_{x0} + \sin \Omega_0 e_{y0},$$

where

$$\begin{aligned} e_{x0} &= \tilde{\mathbf{p}}_{y0} \tilde{L}_{z0} - \tilde{\mathbf{p}}_{z0} \tilde{L}_{y0} - \frac{\tilde{\mathbf{x}}_0}{\tilde{r}_0}, \\ e_{y0} &= \tilde{\mathbf{p}}_{z0} \tilde{L}_{x0} - \tilde{\mathbf{p}}_{x0} \tilde{L}_{z0} - \frac{\tilde{\mathbf{y}}_0}{\tilde{r}_0}, \end{aligned}$$

with

$$\begin{aligned} \tilde{L}_{x0} &= \tilde{\mathbf{y}}_0 \tilde{\mathbf{p}}_{z0} - \tilde{\mathbf{z}}_0 \tilde{\mathbf{p}}_{y0}, \\ \tilde{L}_{y0} &= \tilde{\mathbf{z}}_0 \tilde{\mathbf{p}}_{x0} - \tilde{\mathbf{x}}_0 \tilde{\mathbf{p}}_{z0}. \end{aligned}$$

Since

$$\cos \Omega_0 = \frac{N_{x0}}{N_0} = -\frac{\tilde{L}_{y0}}{\sqrt{\tilde{L}_{x0}^2 + \tilde{L}_{y0}^2}},$$

$$\sin \Omega_0 = \frac{N_{y0}}{N_0} = \frac{\tilde{L}_{x0}}{\sqrt{\tilde{L}_{x0}^2 + \tilde{L}_{y0}^2}},$$

and

$$\tilde{L}_{z0} = \tilde{L}_0 \cos I_0,$$

we find that

$$\tilde{L}_{x0} = \tilde{L}_0 \sin I_0 \sin \Omega_0, \quad \tilde{L}_{y0} = -\tilde{L}_0 \sin I_0 \cos \Omega_0.$$

From the normalized Laplace-Runge-Lenz vector \mathbf{e}_0 , we obtain

$$e_0^2 = [\tilde{\mathbf{p}}_0^2 r_0^2 - (\tilde{\mathbf{p}}_0 \cdot \tilde{\mathbf{r}}_0)^2] \left(\tilde{\mathbf{p}}_0^2 - \frac{2}{r_0} \right) + 1.$$

Hence, when we prepare the initial orbital parameters (e_0 , I_0 , ω_0 , Ω_0), we can provide the initial data of $(\tilde{\mathbf{r}}_0, \tilde{\mathbf{p}}_0)$ for the normalized evolution equations (4.1)–(4.6). Note that since we choose the initial point at the periapsis ($f = 0$ at $\tau = 0$), we find

$$(\tilde{\mathbf{p}}_0 \cdot \tilde{\mathbf{r}}_0) = 0,$$

which can be used to find the initial data.

D. Validity and stability

Before showing our numerical results, we discuss validity of the present approach and the stability conditions. The minimum curvature radius at the radius \mathbf{r}_0 is evaluated as

$$\ell_{\tilde{\mathcal{R}}} \equiv \min[|\tilde{\mathcal{R}}_{\hat{\mu}\hat{\nu}\hat{\rho}\hat{\sigma}}|^{-\frac{1}{2}}, |\tilde{\mathcal{R}}_{\hat{\mu}\hat{\nu}\hat{\rho}\hat{\sigma}\hat{\alpha}}|^{-\frac{1}{3}}, |\tilde{\mathcal{R}}_{\hat{\mu}\hat{\nu}\hat{\rho}\hat{\sigma}\hat{\alpha}\hat{\beta}}|^{-\frac{1}{4}}]$$

$$\sim \min \left[\left(\frac{M}{\mathbf{r}_0^3} \right)^{-\frac{1}{2}}, \left(\frac{M}{\mathbf{r}_0^4} \right)^{-\frac{1}{3}}, \left(\frac{M}{\mathbf{r}_0^5} \right)^{-\frac{1}{4}} \right]$$

$$\sim \mathbf{r}_0 \left(\frac{\mathbf{r}_0}{M} \right)^{1/4}.$$

When we put a binary at $\mathbf{r} = \mathbf{r}_0$, the binary size ℓ_{binary} should satisfy

$$\ell_{\text{binary}} \ll \ell_{\tilde{\mathcal{R}}}.$$

The relativistic effect in a binary is not important when

$$\ell_{\text{binary}} \gg \frac{G(m_1 + m_2)}{c^2}.$$

As for stability of a binary, the mutual gravitational interaction between a binary should be much larger than the tidal force by a third body. The condition is given by

$$\frac{Gm_1 m_2}{r^2} \gg \frac{\mu M}{\mathbf{r}_0^3} r,$$

which corresponds to the condition on the firmness parameter as $\mathfrak{f} \gg 1$. It gives the constraint on a binary size ℓ_{binary} as

$$\ell_{\text{binary}} \ll \left(\frac{m_1 + m_2}{M} \right)^{\frac{1}{3}} \mathbf{r}_0. \quad (4.17)$$

Hence, for a binary with the size of

$$\frac{G(m_1 + m_2)}{c^2} \ll \ell_{\text{binary}} \ll \left(\frac{m_1 + m_2}{M} \right)^{\frac{1}{3}} \mathbf{r}_0,$$

we may apply the present Newtonian approach.

If we are interested in the orbit near the ISCO radius of near extreme Kerr BH ($\mathbf{r}_0 = M$), we find the condition as

$$2 \times 10^{-7} \text{au} \left(\frac{m_1 + m_2}{20M_\odot} \right) \ll \ell_{\text{binary}}$$

$$\ll 6 \times 10^{-3} \text{au} \left(\frac{m_1 + m_2}{20M_\odot} \right)^{\frac{1}{3}} \left(\frac{M}{10^8 M_\odot} \right)^{\frac{2}{3}}.$$

Note that $\ell_{\tilde{\mathcal{R}}} \sim 1 \text{au} (M/10^8 M_\odot)$ in this limit.

We also have another criterion for stability. In order to avoid a chaotic energy exchange instability, we may have to impose the condition for the ratio of the circular radius \mathbf{r}_0 to the binary size ℓ_{binary} such that

$$\frac{\mathbf{r}_0}{\ell_{\text{binary}}} \lesssim C_{\text{chaotic}} \left(\frac{M}{m_1 + m_2} \right)^p,$$

when $M \gg m_1, m_2$. Two parameters in this inequality are evaluated by N -body simulations of two groups [69,70] as

$$C_{\text{chaotic}} \sim 2.8 \quad \text{and} \quad p = \frac{2}{5} \text{ (criterion 1),}$$

$$C_{\text{chaotic}} \sim 5.2 \mathfrak{f}^{\frac{1}{3}} \quad \text{and} \quad p = \frac{1}{3} \text{ (criterion 2).}$$

Here \mathfrak{f} is a complicated function of inner eccentricity e and inclination I such that

$$\mathfrak{f} = 1 - \frac{2}{3} e(1 - e^2) - 0.3 \cos I \left[1 - \frac{e}{2} + 2 \cos I \left(1 - \frac{5}{2} e^{3/2} - \cos I \right) \right].$$

It takes the value in the range of 0 to 2.25, but mostly between 0.6 and 1.0.

Since the above stability condition is only obtained for stellar masses triples and the direct N -body integration is a reliable test of stability in such a setting, we will check such chaotic instability condition in our model.

V. NUMERICAL ANALYSIS

In a hierarchical triple system, there are several important features. One is the so-called vZLK oscillations. If the system is inclined more than some critical angle, there appears an oscillation between the eccentricity and inclination angle. The second interesting feature is an orbital flip, which may appear when the inclination angle evolves into near 90° . The last one which we show is a chaotic feature in the long-time evolution.

Before showing the dynamical evolution of the present system, we first discuss chaotic instability condition in our model.

A. Chaotic instability

In this subsection, we show our results of stability analysis for several values of the initial orbital parameters (the semimajor axis α_0 , eccentricity e_0 , inclination I_0), the circular radius r_0 , and Kerr rotation parameter a . We choose $a = 0.1, 0.3, 0.5, 0.7, 0.9, 0.999M$, $\alpha_0 = 0.005, 0.015, 0.025M$, $e_0 = 0.01, 0.9$ and $I_0 = 0$ (coplanar), 85° . We fix the argument of periapsis and the ascending node as $\omega_0 = 60^\circ$, $\Omega_0 = 30^\circ$ for simplicity.

We perform the simulation until $\tilde{\tau} = 10^4$, which is $\tau = 10^4 n_0 \approx 1600P_0$, where P_0 is initial orbital period of a binary. Since a binary is broken when the system is unstable, we judge stability at the end point of the simulation. However, since the present system is non-integrable and show some chaotic features as we will show later, the boundary values between stability and instability is not sharp. In fact, fixing the orbital parameters of a binary and Kerr parameter a , even when we find a stable orbit for some value of r_0 , we obtain an unstable orbit for a slightly larger value of r_0 . Changing the values of r_0 , the stable and unstable orbits appear randomly. Fortunately, there exists the minimum value of r_0 for stable orbits, below which a binary is broken before $\tilde{\tau} \approx 1000$ (mostly within a few dynamical timescale).

In Fig. 4, we show this minimum value ($r_{0(\text{cr})}$) for given orbital parameters as a reference of chaotic instability. We choose the initial orbital parameters of a binary as the semimajor axis $\alpha_0 = 0.005M$ (dotted line), $0.015M$ (dashed line), and $0.025M$ (thin line). The initial eccentricity e_0 is chosen 0.01 (blue) and 0.9 (red). We fix the other initial orbital parameters as $I_0 = 85^\circ$, $\omega_0 = 60^\circ$, $\Omega_0 = 30^\circ$.

Below the critical radius $r_{0(\text{cr})}$, we always find unstable binary within $\tilde{\tau} = 10^3$. While, beyond the critical radius,

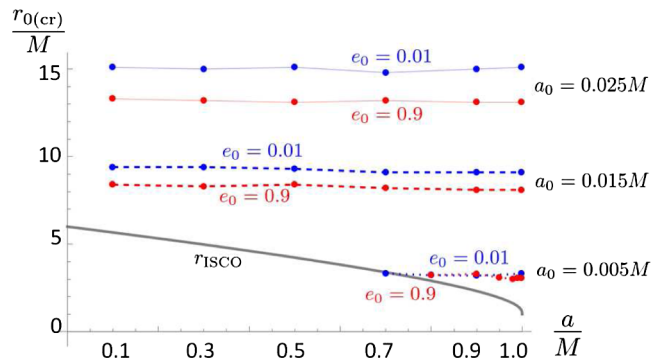


FIG. 4. The minimum radius ($r_{0(\text{cr})}$) in terms of Kerr rotation parameter a for given values of the semimajor axis $\alpha_0 = 0.025M$ (thin line), $0.015M$ (dashed line), $0.005M$ (dotted line). The blue and red correspond to the cases of the initial eccentricity $e_0 = 0.01$ and 0.9 , respectively. We fix the other initial orbital parameters as $e_0 = 0.01, I_0 = 85^\circ, \omega_0 = 60^\circ, \Omega_0 = 30^\circ$. Below the critical radius $r_{0(\text{cr})}$, we always find unstable binary. Beyond the critical radius, stable orbits and unstable ones appear randomly. We also show the ISCO radius (black), below which the circular orbit of the c.m. becomes unstable.

stable and unstable orbits appear randomly. In this case, however, unstable orbit can evolve beyond $\tilde{\tau} = 10^3$, but a binary is broken before $\tilde{\tau} = 10^4$. Since the instability appears after many orbital cycles, it is not dynamical instability but may be caused by chaotic instability. It is consistent with the fact that stable and unstable orbits appear randomly beyond the critical radius. The appearance of unstable orbits becomes less frequent as r_0 increases. We expect that the system becomes much stable when r_0 is large enough as we show later.

Figure 4 shows that the critical radius $r_{0(\text{cr})}$ is almost independent of the Kerr parameter a . We also find that its dependence on the initial eccentricity is rather small. The compactness of a binary (the initial semimajor axis α_0) is the most important factor. We find that the more compact binary can have stable orbits closer to SMBH. In fact, a stable binary with $\alpha_0 = 0.005M$ can exist near the ISCO radius.

The inclination dependence is also important as shown in Fig. 5, in which we include the coplanar cases ($I_0 = 0^\circ$). The green and magenta colored lines correspond to the cases with the initial eccentricity $e_0 = 0.01$ and 0.9 , respectively.

Figure 5 shows that the critical radius in the coplanar case is smaller than that in the highly inclined orbit. The coplanar binary is more stable than the highly inclined binary. It may be because the vZLK oscillation appears in the highly inclined orbit.

As we discussed in Sec. IV D, the criterion of chaotic instability of three body system can be described by two parameters, C_{chaotic} and p . In the present model, we can also evaluate those parameters. We find $p = 1/3$ and $C_{\text{chaotic}} = \tilde{f}_{(\text{cr})}^{1/3}$, because the critical value of the firmness parameter \tilde{f} depend slightly on the initial eccentricity e_0 and

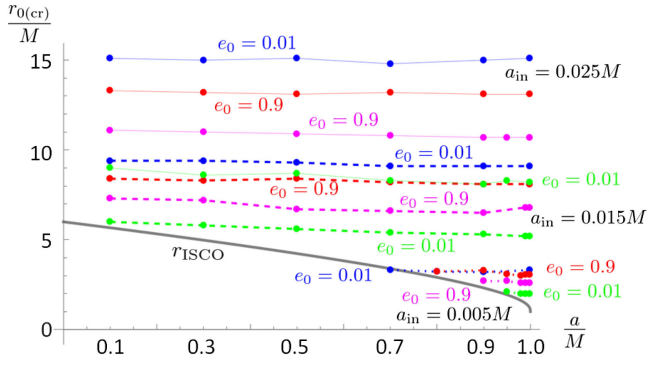


FIG. 5. The critical radius ($r_{0(\text{cr})}$) in terms of Kerr rotation parameter a for given values of the semimajor axis $\alpha_0 = 0.025M$ (thin line), $0.015M$ (dashed line), $0.005M$ (dotted line). We add the coplanar cases ($I_0 = 0^\circ$) in Fig. 4. The green and magenta colored lines correspond to the cases of the initial eccentricity $e_0 = 0.01$ and 0.9 , respectively. We fix the other initial orbital parameters as $\omega_0 = 60^\circ$, $\Omega_0 = 30^\circ$.

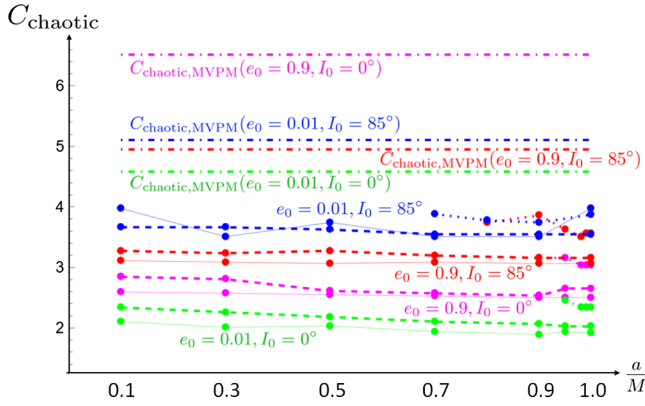


FIG. 6. C_{chaotic} is shown for various values of the parameters. The colors and types of lines denote the same models as those in Fig. 5. The values of C_{chaotic} for the highly inclined orbits is larger than those for the coplanar orbits. As references, we also show the values of C_{chaotic} in criterion 2 by the dot-dashed lines.

inclination I_0 , but are almost independent of the other parameters, which means criterion 2 is more suitable to the present model. We show our results of C_{chaotic} in Fig. 6.

The values of C_{chaotic} for the highly inclined orbits is always larger than those for the coplanar orbits. The values of C_{chaotic} in our model is always smaller than those in the criterion 2, which is given by Mylläri *et al.* (MVPM) [70]. However, since the system is chaotic near C_{chaotic} , there is no clear critical value. In fact, a binary with some initial data with the firmness $\mathfrak{f} > \mathfrak{f}_{\text{cr}} \equiv C_{\text{chaotic}}^3$ shows instability. In this sense, our result is consistent with criterion 2.

B. vZLK oscillations

In a hierarchical triple system, when the inclination is larger than some critical angle, a stable binary orbit shows vZLK oscillations. We present four typical models, which

TABLE I. Parameters of the models. The Kerr rotation parameter a , the argument of periapsis ω_0 , and the ascending node Ω_0 are fixed.

Model	a/M	α_0/M	r_0/M	e_0	I_0	ω_0	Ω_0
I	0.9	0.005	10	0.01	85°	60°	30°
II	0.9	0.005	2.9	0.01	60°	60°	30°
III	0.9	0.005	3.2	0.01	85°	60°	30°
IV	0.9	0.015	10	0.01	85°	60°	30°

are listed in Table I, in order to clarify the important properties of vZLK oscillations.

1. Regular vZLK oscillations

We first show Model I as an example of the regular vZLK oscillations in Fig. 7. We choose the Kerr rotation parameter as $a = 0.9M$, the initial orbital parameters of a binary as $\alpha_0 = 0.005M$, $e_0 = 0.01$, $I_0 = 85^\circ$, $\omega_0 = 60^\circ$, $\Omega_0 = 30^\circ$, and the circular radius as $r_0 = 10M$.

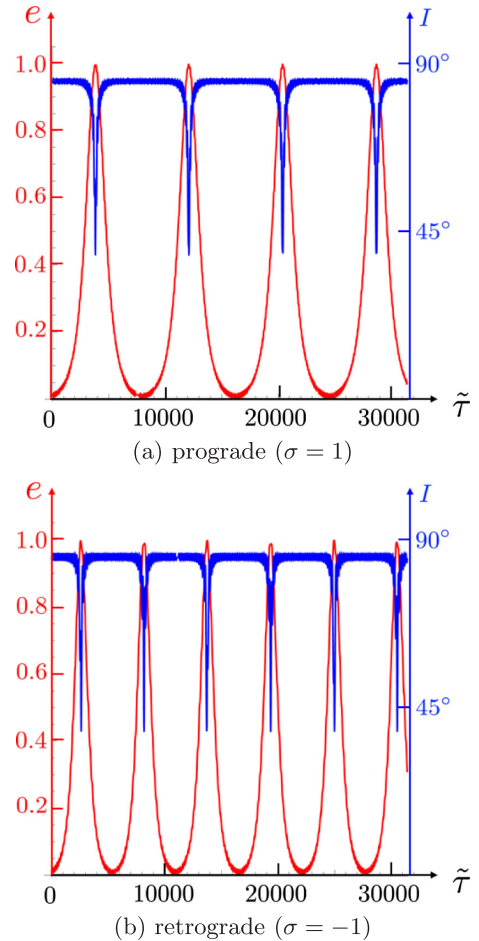


FIG. 7. Time evolution of the eccentricity e and inclination angle I with $\alpha_0 = 0.005M$ and $r_0 = 10M$ (Model I) [(a) prograde orbit, (b) retrograde orbit]. The Kerr parameter is $a = 0.9M$, and the other initial orbital parameters of a binary are $e_0 = 0.01$, $I_0 = 85^\circ$, $\omega_0 = 60^\circ$, and $\Omega_0 = 30^\circ$.

We can clearly see the vZLK oscillations (a periodic exchange between the eccentricity e and inclination I). The eccentricity can reach almost unity. Since the critical radius for $\alpha_0 = 0.005M$ is $r_{0(\text{cr})} = 3.2M$, this model with $r_0 = 10M$ should be highly stable. In fact, as shown in Fig. 7, the oscillations are highly regular.

2. Comparison with the double-averaging approach

In Newtonian hierarchical triple system, one sometimes use the double-averaging (DA) approach, in which we take averages of the Lagrange planetary equations over two orbital periods and analyze the averaged equations for the orbital parameters in order to find their long-time behaviors. In Appendix B, we discuss the planetary equations in the present models and analyze the DA equations.

In the present Model I, the DA approach gives very good approximation as shown in Fig. 8, which is the result for the prograde orbit. We also find the almost same figures for the retrograde orbit.

3. Oscillation period

One of the important properties of vZLK oscillations for observation is the oscillation period T_{vZLK} . For Newtonian vZLK oscillations. It is approximately given by

$$T_{\text{vZLK}} \sim \frac{P_{\text{out}}^2}{P_{\text{in}}} = \frac{(m_1 + m_2)}{M} \left(\frac{r_0}{\alpha_0} \right)^3 P_{\text{in}} = \bar{f} P_{\text{in}}.$$

As we discussed in the previous subsection, when we find regular vZLK oscillations, the DA approach gives a good approximation. Using the DA approximation, we can easily evaluate the oscillation period analytically as shown in Appendix B. It shows that the relativistic effects reduce the vZLK timescale by a factor 0.1–0.25.

One interesting observation in Fig. 7 is that the oscillation period for the retrograde orbit is smaller than that for the prograde orbit. It is confirmed by Fig. 14 obtained by the DA approach.

4. Critical inclination angle

The critical inclination angle, beyond which the vZLK oscillation occurs, can be obtained by evaluating the maximum value of the eccentricity, e_{max} , in the models with very small initial eccentricity.

In Fig. 9, we show e_{max} in terms of the initial inclination angle I_0 . We choose $e_0 = 0.01$, $\alpha_0 = 0.005M$ and $r_0 = 10M$ to find regular vZLK oscillations. The solid curve denotes e_{max} obtained by the DA approximation. Although we show the case of $a = 0.9M$ in Fig. 9, the results do not depend on a at all. This figure shows that the critical inclination angle is a little less than 40° .

The direct integration gives a little bit smaller value of the critical inclination angle than the DA approximation, but the DA scheme is not too contrasting. In the extreme limit such that $r_0 \rightarrow r_{\text{ISCO}}$ as well as $a \rightarrow M$, the larger critical inclination angle such as 60° could be found as discussed in Appendix 2 c. However, it turns out that when we restrict to stable binary orbits, the critical value is much smaller even in the extreme limit. This is confirmed by the direct integration (red dots in Fig. 16), which provides almost the same as Fig. 9.

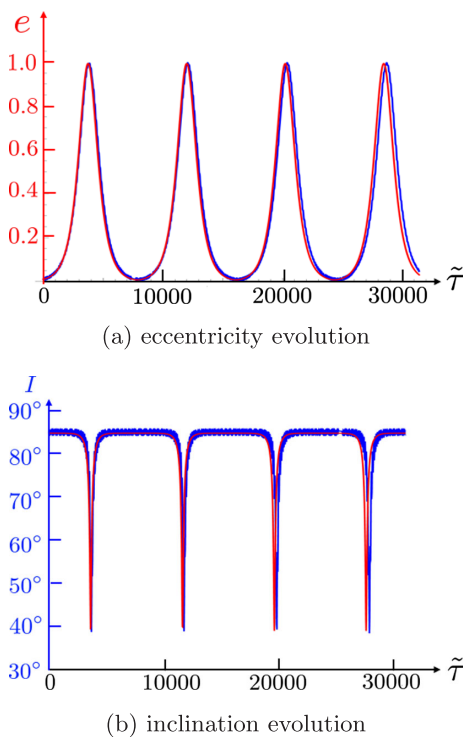


FIG. 8. Comparison of the direct integration (blue) and the double-averaging approximation (red) of (a) the eccentricity e and (b) inclination angle I . The model is the same model as that in Fig. 7. The results are completely overlapped.

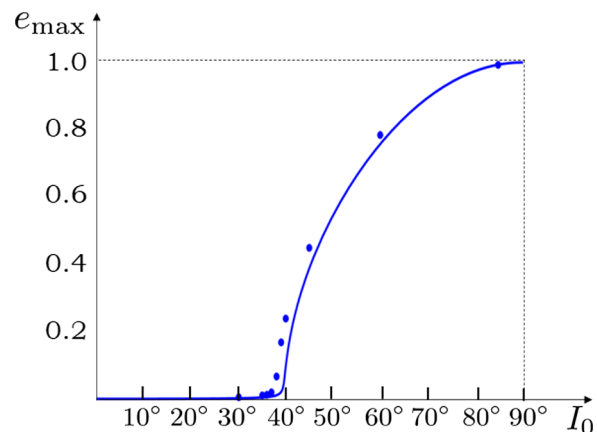


FIG. 9. The maximum value of the eccentricity in vZLK oscillations in terms of the initial inclination angle I_0 . We assume $e_0 = 0.01$, $\alpha_0 = 0.005M$, $r_0 = 10M$, and $a = 0.9M$. The solid curve denotes e_{max} obtained by the DA approximation.

C. Chaotic features

Since a three-body system is nonintegrable, we may find chaotic features in binary orbits, especially near the critical boundary between stable and unstable orbits. As we discussed in Sec. VA, there exists a critical radius $r_{0(\text{cr})}$ for given orbital parameters of a binary, below which a binary is broken before $\tilde{\tau} = 10^3$. We then expect some chaotic features appear in a stable binary orbit with a slightly larger radius than $r_{0(\text{cr})}$. Here we give three models (Model II, Model III, and Model IV) listed in Table I.

In Model II, we change the circular radius r_0 from $10M$ (Model I) to the critical radius $r_{0(\text{cr})} = 2.9M$ as well as the initial inclination angle I_0 from 85° to 60° , while in Model III we change only the circular radius r_0 from $10M$ to $r_{0(\text{cr})} = 3.2M$. In Model IV, we change only the semimajor axis a_0 from $0.005M$ in Model I to $0.015M$. In Model II and Model III, the parameters are just on the critical boundary for chaotic instability, while in Model IV, they are near the instability boundary.

We find two typical chaotic features in those models: irregular vZLK oscillations and orbital flip.

1. Irregular oscillations

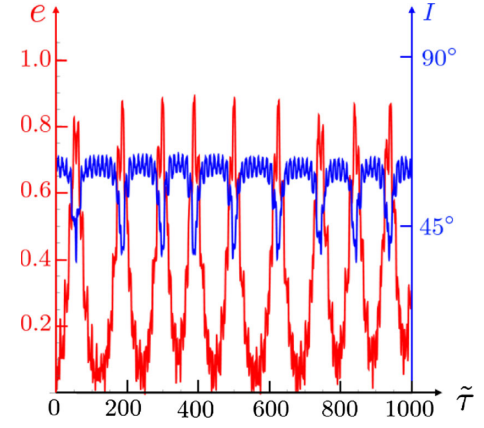
In Fig. 10, we show time evolution of the eccentricity (red curve) and inclination (blue curve). We find the vZLK oscillations are stable but quite irregular. We can easily find that the oscillation period is not constant in Fig. 10(b). We also see that the maximum and minimum values of the eccentricities are changing in time.

Since the oscillation period looks regular, Model IV is less chaotic than Model II and Model III. It is because $r_0 = 10M$ of Model IV is slightly larger than the critical radius $r_{0(\text{cr})} = 9.1M$ for $a_0 = 0.015M$, while the parameters of Model II and Model III are just on the critical boundary for chaotic instability.

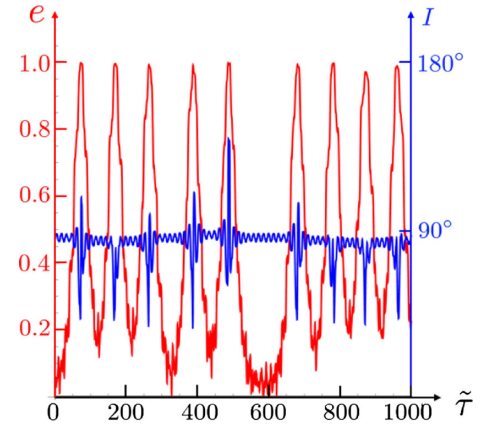
2. Orbital flip

When the initial inclination angle is close to 90° , we may expect a phenomenon of orbital flip, in which the inclination angle will evolve beyond 90° . We do not find such phenomenon when the initial inclination angle is not so large, e.g., $I_0 = 60^\circ$ as shown in Fig. 10(a). Even when the initial inclination angle is close to 90° , the orbital flip does not occur in regular vZLK oscillations as shown in Fig. 7.

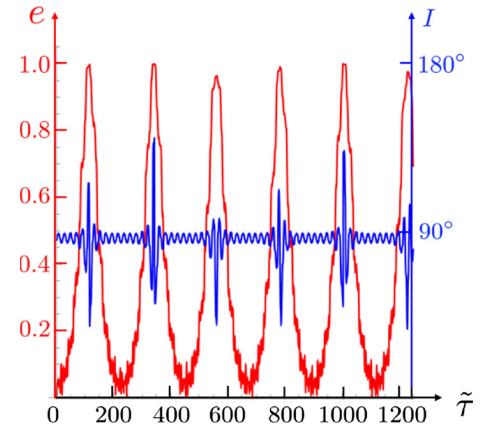
When the initial inclination angle is close to $I_0 = 90^\circ$ and the vZLK oscillations are chaotic (Model III and Model IV), we find the orbital flips as shown in Figs. 10(b) and (c). Although it is quite random when the orbital flip occurs, it happens when the eccentricity gets large. It is interesting because in a regular vZLK oscillations, the eccentricity is larger when the inclination angle becomes smaller, while in the orbital flip models, the eccentricity becomes very large not only when the



(a) Model II



(b) Model III



(c) Model IV

FIG. 10. Time evolution of eccentricity and inclination for (a) Model II, (b) Model III, and (c) Model IV, respectively. The model parameters are given in Table I.

inclination angle becomes smaller but also when the inclination angle goes beyond 90° . Our results align with the outcomes reported in the Newtonian (or 1PN) triple system study by Naoz *et al.* [71].

D. Rotation dependence

As we mentioned before, the properties of dynamics of a binary are little dependent of a SMBH rotation parameter a when the circular radius r_0 and the initial semimajor axis a_0 are fixed. It is because the Riemann curvature on the equatorial plane only depends on r_0 just as Schwarzschild BH and the procession frequency ω_P at the fixed r_0 very weakly depends on a as shown in Fig. 3.

However, the ISCO radius, below which the c.m. of a binary becomes unstable as shown in Appendix A, highly depends on a . As a result, a highly compact binary can exist at more inner circular radius for a more rapidly rotating SMBH. In the top figure of Fig. 11, We show the critical semimajor axis $a_{0(\text{cr})}$ below which a binary is stable. The circular radius is chosen at $r_0 = r_{\text{ISCO}}$. The initial eccentricity is $e_0 = 0.01$, while the initial inclination angle is chosen as $I_0 = 0$ (coplanar) and $I_0 = 85^\circ$. The coplanar case ($I_0 = 0$) is shown by black curves. Since it is a regular orbit, the boundary between stable and unstable orbit is clear. On the other hand, in highly inclined case ($I_0 = 85^\circ$),

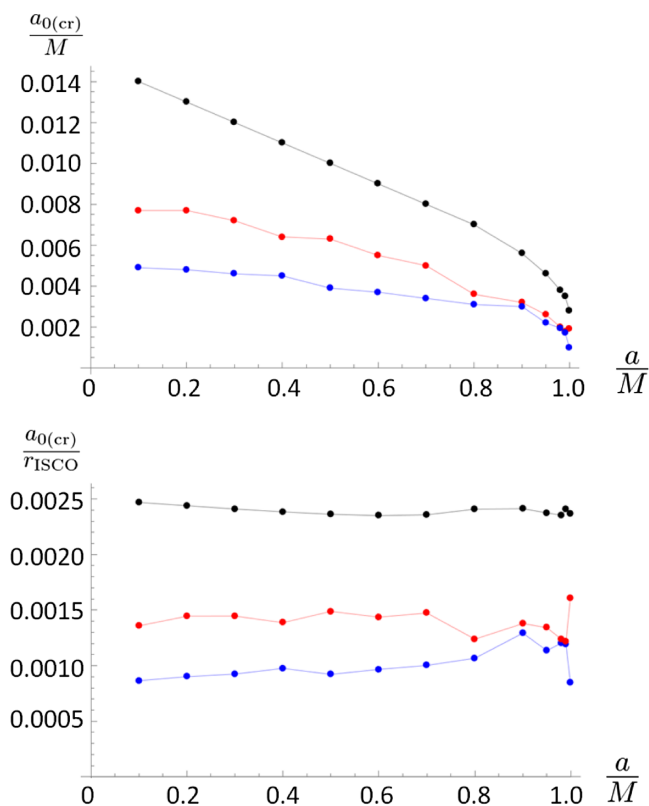


FIG. 11. (Top) Critical semimajor axis $a_{0(\text{cr})}$ at r_{ISCO} in terms of the Kerr rotation parameter a . (Bottom) $a_{0(\text{cr})}/r_{\text{ISCO}}$ in terms of a . The initial eccentricity is $e_0 = 0.01$, while the initial inclination angle are chosen as $I_0 = 0$ (black) and $I_0 = 85^\circ$ (red and blue). For the coplanar case ($I_0 = 0$), all orbits are stable below black curves. For $I_0 = 85^\circ$, all orbits are stable below blue curves, while there exist stable and unstable orbits between blue curves and red curves.

since the system is chaotic, stability highly depends on the initial conditions. As a result, there are two critical radii; one is that all orbits are stable below some critical radius (blue curves), and the other is that there exist stable and unstable orbits between blue curves and another critical radius (red curves).

In the bottom figure of Fig. 11, we show $a_{0(\text{cr})}/r_{\text{ISCO}}$, which is little dependent on the Kerr rotation parameter a . In the extreme limit of $a \rightarrow M$, there appears strange behaviors especially for $I_0 = 85^\circ$. It is because ω_P becomes very large near the ISCO radius (see Fig. 2).

VI. SUMMARY AND DISCUSSION

In this paper, we discuss dynamics of a binary system orbiting around a rotating SMBH. Assuming an observer rotating on a nearly circular orbit around a Kerr SMBH, we write down the equations of motion of a binary in the observer's local inertial frame. Using Fermi-Walker transport with small acceleration, which removes the interaction terms between the c.m. of a binary and its relative coordinates, we set up Newtonian self-gravitating system in the local proper reference frame. As a result, the c.m. of a binary follows the observer's orbit, but its motion deviates from an exact geodesic. Since the relative motion is decoupled from the system, we first solve it, and then find the motion of the c.m. by the perturbation equations with the small acceleration, which is given by the relative motion.

To present our results, we first discuss the stability conditions. In the hierarchical triple system, there are two widely used criteria for chaotic instability, which are evaluated by N -body simulations by two independent groups [69,70]. The criterion given by [70] fits our model because the dependence of mass parameter is the same as $p = 1/3$. The critical value for chaotic instability (C_{chaotic}) in our model is slightly smaller than the result by [70]. However, the system is chaotic near C_{chaotic} , there is no clear critical value. In fact, a binary with some initial data with the firmness $\bar{f} > \bar{f}_{\text{cr}} \equiv C_{\text{chaotic}}^3$ shows instability. In this sense, our result is consistent with that by [70].

We then analyze the properties of stable vZLK oscillations. Although we show the result only for the case of $a = 0.9M$, the behaviors of a binary are almost the same when we fix the circular radius r_0 and the initial semimajor axis a_0 .

For highly compact binaries with large firmness parameter ($\bar{f} \gg \bar{f}_{\text{cr}}$), the vZLK oscillations is quite regular and stable. The double-averaging method gives a good approximation in this parameter space. The critical inclination angle for vZLK oscillations is about 40° , which is also almost independent of the rotation parameter a .

For the binary with the firmness parameter slightly larger than the critical value ($\bar{f} \gtrsim \bar{f}_{\text{cr}}$), since the system is chaotic, we find chaotic vZLK oscillations, which become irregular both in the oscillation period and in the amplitude. If the

initial inclination is large, we find an orbital flip, which also appears randomly.

In this paper, we assume that the c.m. of a binary moves along an almost circular orbit, but an eccentric orbit is interesting to be studied since the vZLK oscillation may be modulated on a longer timescale [72–76]. However, for such a highly eccentric orbit, the present proper reference frame expanded up to the second order of the spatial coordinates $x^{\hat{a}}$ may not be sufficient. We may need higher-order terms in the metric, where the derivatives of the Riemann curvature appear [53,54]. Although the basic equations are very complicated, such an extension is straightforward.

Our future work will involve evaluating the GWs from the present hierarchical triple setting using the black hole perturbation approach, since near the ISCO radius the quadrupole formula may not be valid [77].

ACKNOWLEDGMENTS

We thank Luc Blanchet, Vitor Cardoso, Ericourgoulhon, and Haruka Suzuki for useful discussions. This work was supported in part by JSPS KAKENHI Grants No. JP17H06359, No. JP19K03857 (K. M.), and by Grant No. JP20K03953 (H. O.). P. G. acknowledges support from C. V. Raman fellowship grant. K. M. would like to acknowledge the Yukawa Institute for Theoretical Physics at Kyoto University, where the present work

was begun during the Visitors Program of FY2022. He would also thank Niels Bohr Institute/Niels Bohr International Academy, The Max Planck Institute for Gravitational Physics (Albert Einstein Institute), The laboratory AstroParticle and Cosmology (APC), and CENTRA/ Instituto Superior Técnico, where most of this work was performed.

APPENDIX A: MOTION WITH 0.5 PN CORRECTION TERM

As we discussed in the text, in order to analyze the motion of the c.m. of a binary system, we have to consider 0.5 PN terms. As shown before, we can assume $\mathbf{R} = 0$ by introduction of the acceleration given by Eq. (2.12). We first solve the relative coordinates \mathbf{r} , and then the motion of the observer (or the c.m.).

1. Equations of motion for relative coordinates

The equation of motion for relative coordinates \mathbf{r} of a binary is now given by

$$\tilde{\mathcal{L}}_{\text{rel}}(\mathbf{r}, \dot{\mathbf{r}}) = \mathcal{L}_{\text{rel}}(\mathbf{r}, \dot{\mathbf{r}}) + \mathcal{L}_{1/2\text{-rel}}(\mathbf{r}, \dot{\mathbf{r}}),$$

where \mathcal{L}_{rel} is given by Eq. (3.9), while

$$\begin{aligned} \mathcal{L}_{1/2\text{-rel}}(\mathbf{r}, \dot{\mathbf{r}}) &= -\mu \frac{2(m_1 - m_2)}{3(m_1 + m_2)} (\bar{\mathcal{R}}_{\hat{0}\hat{x}\hat{y}\hat{x}} x(\dot{x}y - y\dot{x}) + \bar{\mathcal{R}}_{\hat{0}\hat{z}\hat{y}\hat{z}} z(\dot{z}y - y\dot{z})) \\ &= -\mu \frac{2(m_1 - m_2)M}{(m_1 + m_2)\mathbf{r}_0^3} \frac{\sqrt{\Delta(\mathbf{r}_0)}(\sigma\sqrt{M\mathbf{r}_0} - a)}{F_\sigma^2(\mathbf{r}_0)} (-x(\dot{x}y - y\dot{x}) + z(\dot{z}y - y\dot{z})). \end{aligned}$$

In nonrotating Fermi-Walker coordinates, we find \mathcal{L}_{rel} is given by Eq. (3.10), while

$$\begin{aligned} \mathcal{L}_{1/2\text{-rel}}(\mathbf{r}, \dot{\mathbf{r}}) &= \mu \frac{2(m_1 - m_2)M}{(m_1 + m_2)\mathbf{r}_0^3} \frac{\sqrt{\Delta(\mathbf{r}_0)}(\sigma\sqrt{M\mathbf{r}_0} - a)}{F_\sigma^2(\mathbf{r}_0)} \\ &\quad \times \{ \cos \sigma \mathfrak{w}_R \tau [x(\dot{x}y - y\dot{x}) + z(\dot{y}z - z\dot{y}) + \mathfrak{w}_R x(x^2 + y^2 - z^2)] \\ &\quad - \sin \sigma \mathfrak{w}_R \tau [y(\dot{x}y - y\dot{x}) + z(\dot{z}x - x\dot{z}) + \mathfrak{w}_R y(x^2 + y^2 - z^2)] \}. \end{aligned}$$

The momentum is obtained from the Lagrangian $\tilde{\mathcal{L}}_{\text{rel}}(\mathbf{r}, \dot{\mathbf{r}})$ as

$$\begin{aligned} p_x &= \mu \dot{x} + \mu \mathfrak{w}_P y + \mu \frac{2(m_1 - m_2)M}{(m_1 + m_2)\mathbf{r}_0^3} \frac{\sqrt{\Delta(\mathbf{r}_0)}(\sigma\sqrt{M\mathbf{r}_0} - a)}{F_\sigma^2(\mathbf{r}_0)} (-xy \cos \sigma \mathfrak{w}_R \tau + (y^2 - z^2) \sin \sigma \mathfrak{w}_R \tau), \\ p_y &= \mu \dot{y} - \mu \mathfrak{w}_P x + \mu \frac{2(m_1 - m_2)M}{(m_1 + m_2)\mathbf{r}_0^3} \frac{\sqrt{\Delta(\mathbf{r}_0)}(\sigma\sqrt{M\mathbf{r}_0} - a)}{F_\sigma^2(\mathbf{r}_0)} (-xy \sin \sigma \mathfrak{w}_R \tau + (x^2 - z^2) \cos \sigma \mathfrak{w}_R \tau), \\ p_z &= \mu \dot{z} + \mu \frac{2(m_1 - m_2)M}{(m_1 + m_2)\mathbf{r}_0^3} \frac{\sqrt{\Delta(\mathbf{r}_0)}(\sigma\sqrt{M\mathbf{r}_0} - a)}{F_\sigma^2(\mathbf{r}_0)} z(y \cos \sigma \mathfrak{w}_R \tau + x \sin \sigma \mathfrak{w}_R \tau). \end{aligned}$$

The Hamiltonian is given by

$$\tilde{\mathcal{H}}_{\text{rel}}(\mathbf{r}, \mathbf{p}) = \mathcal{H}_{\text{rel}}(\mathbf{r}, \mathbf{p}) + \mathcal{H}_{1/2\text{-rel}}(\mathbf{r}, \mathbf{p}),$$

where $\mathcal{H}_{\text{rel}}(\mathbf{r}, \mathbf{p})$ is given by Eq. (3.11), while

$$\begin{aligned} \mathcal{H}_{1/2\text{-rel}}(\mathbf{r}, \mathbf{p}) = & -\frac{2\mu(m_1 - m_2)^2 M^2 \Delta(\mathbf{r}_0)(\sigma\sqrt{M\mathbf{r}_0} - a)^2}{(m_1 + m_2)^2 \mathbf{r}_0^6 F_\sigma^4(\mathbf{r}_0)} [(-\mathbf{x}\mathbf{y} \cos \sigma\mathbf{w}_R \tau + (\mathbf{y}^2 - \mathbf{z}^2) \sin \sigma\mathbf{w}_R \tau)^2 \\ & + (-\mathbf{x}\mathbf{y} \sin \sigma\mathbf{w}_R \tau + (\mathbf{x}^2 - \mathbf{z}^2) \cos \sigma\mathbf{w}_R \tau)^2 + \mathbf{z}^2(\mathbf{y} \cos \sigma\mathbf{w}_R \tau + \mathbf{x} \sin \sigma\mathbf{w}_R \tau)^2]. \end{aligned}$$

This Hamiltonian is complicated, but it should not be considered because it is beyond quadrupole approximation, although the momenta of the particles are modified. For an equal mass binary ($m_1 = m_2$), the 0.5 PN correction term vanishes and the momenta are also the same as the Newtonian ones. As a result, the Newtonian solution is also valid.

2. Motion of the center of mass of a binary and its stability

In order to study stability of the c.m. of a binary system, we analyze Eq. (2.12). Since \mathbf{R} is measured by the circular observer at $\mathbf{r} = \mathbf{r}_0$, we can split the 4-velocity u^μ as

$$u^\mu = u_{(0)}^\mu + u_{(1)}^\mu,$$

where

$$\begin{aligned} u_{(0)}^\mu &= \frac{d\mathbf{x}_{(0)}^\mu}{d\tau} = (u_{(0)}^0, 0, 0, u_{(0)}^3) = \frac{1}{\mathbf{r}_0 F_\sigma(\mathbf{r}_0)} (\mathbf{r}_0^2 + a\sigma\sqrt{M\mathbf{r}_0}, 0, 0, \sigma\sqrt{M\mathbf{r}_0}), \\ u_{(1)}^\mu &= \frac{d\mathbf{x}_{(1)}^\mu}{d\tau}, \end{aligned}$$

with

$$\begin{aligned} \mathbf{x}_{(0)}^\mu &= \left(\frac{\mathbf{r}_0^2 + a\sigma\sqrt{M\mathbf{r}_0}}{\mathbf{r}_0 F_\sigma(\mathbf{r}_0)} \tau, \mathbf{r}_0, \frac{\pi}{2}, \frac{\sigma\sqrt{M\mathbf{r}_0}}{\mathbf{r}_0 F_\sigma(\mathbf{r}_0)} \tau \right), \\ \mathbf{x}_{(1)}^\mu &\equiv e^\mu{}_\nu R^\nu. \end{aligned}$$

The acceleration a^μ is given by the motion of a binary $x^{\hat{\mu}}(\tau)$ in a rotating frame as

$$\begin{aligned} a^\mu &= \frac{6\mu}{m_1 + m_2} \frac{\sqrt{\Delta}(\sigma\sqrt{M\mathbf{r}_0} - a) M}{F_\sigma^2(\mathbf{r}_0) \mathbf{r}_0^3} \left[\delta_1^\mu \frac{\sqrt{\Delta}}{\mathbf{r}_0} \dot{y}x + \delta_2^\mu \frac{1}{\mathbf{r}_0} \dot{y}z \right. \\ & \left. + \frac{1}{\mathbf{r}_0 F_\sigma(\mathbf{r}_0) \sqrt{\Delta}} (\delta_0^\mu \sigma\sqrt{M\mathbf{r}_0} (\mathbf{r}_0^2 + a^2 - 2a\sigma\sqrt{M\mathbf{r}_0}) + \delta_3^\mu (\mathbf{r}_0^2 - 2M\mathbf{r}_0 + a\sigma\sqrt{M\mathbf{r}_0})) (-\dot{x}x + \dot{z}z) \right]. \end{aligned}$$

Here, we assume that the deviation from a circular orbit is small, i.e., $\mathbf{x}_{(1)}^\mu$ and $u_{(1)}^\mu$ are small perturbations. Ignoring nonlinear deviation terms in the equations of motion $\frac{D u_{(1)}^\mu}{d\tau} = a^\mu$, because the circular orbit $\mathbf{x}_{(0)}^\mu(\tau)$ is a geodesic, we obtain a linear differential equation as

$$\frac{d u_{(1)}^\mu}{d\tau} + 2\Gamma_{\rho\sigma}^\mu(\mathbf{r}_0) u_{(0)}^\rho u_{(1)}^\sigma + \frac{\partial \Gamma_{\rho\sigma}^\mu}{\partial \mathbf{x}^\alpha}(\mathbf{r}_0) \mathbf{x}_{(1)}^\alpha u_{(0)}^\rho u_{(0)}^\sigma = a^\mu,$$

where a^μ acts as an external force. Describing the deviation as

$$\mathbf{x}_{(1)}^\mu = (\mathbf{t}_{(1)}, \mathbf{r}_{(1)}, \theta_{(1)}, \varphi_{(1)}),$$

we find

$$\begin{aligned} \frac{d^2 \mathbf{t}_{(1)}}{d\tau^2} + \frac{2M}{\mathbf{r}_0 \Delta(\mathbf{r}_0) F_\sigma(\mathbf{r}_0)} (\mathbf{r}_0^2 + a^2 - 2a\sigma\sqrt{M\mathbf{r}_0}) \frac{d\mathbf{r}_{(1)}}{d\tau} \\ = a^0 = -\frac{6\mu}{m_1 + m_2} \frac{M}{\mathbf{r}_0^4 F_\sigma^3(\mathbf{r}_0)} (M\mathbf{r}_0 - a\sigma\sqrt{M\mathbf{r}_0}) (\mathbf{r}_0^2 + a^2 - 2a\sigma\sqrt{M\mathbf{r}_0}) (\dot{x}x - \dot{z}z), \end{aligned} \quad (\text{A1})$$

$$\begin{aligned} \frac{d^2 \mathbf{r}_{(1)}}{d\tau^2} - \frac{3M\Delta(\mathbf{r}_0)}{\mathbf{r}_0^3 F_\sigma^2(\mathbf{r}_0)} \mathbf{r}_{(1)} + \frac{2M\Delta(\mathbf{r}_0)}{\mathbf{r}_0^3 F_\sigma(\mathbf{r}_0)} \frac{d\mathbf{t}_{(1)}}{d\tau} - \frac{2\Delta(\mathbf{r}_0)}{\mathbf{r}_0^3 F_\sigma(\mathbf{r}_0)} (Ma + \sigma\mathbf{r}_0\sqrt{M\mathbf{r}_0}) \frac{d\varphi_{(1)}}{d\tau} \\ = a^1 = \frac{6\mu}{m_1 + m_2} \frac{M\Delta(\sigma\sqrt{M\mathbf{r}_0} - a)}{\mathbf{r}_0^4 F_\sigma^2(\mathbf{r}_0)} xy, \end{aligned} \quad (\text{A2})$$

$$\frac{d^2 \theta_{(1)}}{d\tau^2} + \frac{M}{\mathbf{r}_0^3 F_\sigma^2(\mathbf{r}_0)} (\mathbf{r}_0^2 + 3a^2 - 4a\sigma\sqrt{M\mathbf{r}_0}) \theta_{(1)} = a^2 = \frac{6\mu}{m_1 + m_2} \frac{M\sqrt{\Delta}(\sigma\sqrt{M\mathbf{r}_0} - a)}{\mathbf{r}_0^4 F_\sigma^2(\mathbf{r}_0)} zy, \quad (\text{A3})$$

$$\begin{aligned} \frac{d^2 \varphi_{(1)}}{d\tau^2} + \frac{2}{\mathbf{r}_0 \Delta(\mathbf{r}_0) F_\sigma(\mathbf{r}_0)} (Ma + \sigma\sqrt{M\mathbf{r}_0}(\mathbf{r}_0 - 2M)) \frac{d\mathbf{r}_{(1)}}{d\tau} \\ = a^3 = -\frac{6\mu}{m_1 + m_2} \frac{M}{\mathbf{r}_0^4 F_\sigma^3(\mathbf{r}_0)} (\sigma\sqrt{M\mathbf{r}_0} - a) (\mathbf{r}_0^2 - 2M\mathbf{r}_0 + a\sigma\sqrt{M\mathbf{r}_0}) (\dot{x}x - \dot{z}z), \end{aligned} \quad (\text{A4})$$

Integrating Eqs. (A1) and (A4), we obtain

$$\begin{aligned} \frac{d\mathbf{t}_{(1)}}{d\tau} = -\frac{2M}{\mathbf{r}_0 \Delta(\mathbf{r}_0) F_\sigma(\mathbf{r}_0)} (\mathbf{r}_0^2 + a^2 - 2a\sigma\sqrt{M\mathbf{r}_0}) \mathbf{r}_{(1)} \\ - \frac{3\mu}{m_1 + m_2} \frac{M}{\mathbf{r}_0^4 F_\sigma^3(\mathbf{r}_0)} (M\mathbf{r}_0 - a\sigma\sqrt{M\mathbf{r}_0}) (\mathbf{r}_0^2 + a^2 - 2a\sigma\sqrt{M\mathbf{r}_0}) (x^2 - z^2), \end{aligned} \quad (\text{A5})$$

$$\begin{aligned} \frac{d\varphi_{(1)}}{d\tau} = -\frac{2}{\mathbf{r}_0 \Delta(\mathbf{r}_0) F_\sigma(\mathbf{r}_0)} (Ma + \sigma\sqrt{M\mathbf{r}_0}(\mathbf{r}_0 - 2M)) \mathbf{r}_{(1)} \\ - \frac{3\mu}{m_1 + m_2} \frac{M}{\mathbf{r}_0^4 F_\sigma^3(\mathbf{r}_0)} (\sigma\sqrt{M\mathbf{r}_0} - a) (\mathbf{r}_0^2 - 2M\mathbf{r}_0 + a\sigma\sqrt{M\mathbf{r}_0}) (x^2 - z^2), \end{aligned} \quad (\text{A6})$$

where we set the integration constants as zero. Plugging Eqs. (A5) and (A6) into Eq. (A2), we obtain the perturbation equation for the radial coordinates $\mathbf{r}_{(1)}$ as

$$\frac{d^2 \mathbf{r}_{(1)}}{d\tau^2} + k_{\mathbf{r}}^2 \mathbf{r}_{(1)} + A(x^2 - z^2) + B\dot{y}x = 0, \quad (\text{A7})$$

where

$$k_{\mathbf{r}}^2 \equiv \frac{M}{\mathbf{r}_0^3 F_\sigma^2(\mathbf{r}_0)} (\mathbf{r}_0^2 - 6M\mathbf{r}_0 - 3a^2 + 8a\sigma\sqrt{M\mathbf{r}_0}) \quad (\text{A8})$$

$$A \equiv \frac{6\mu M\Delta}{(m_1 + m_2)\mathbf{r}_0^5 F_\sigma^4(\mathbf{r}_0)} (\mathbf{r}_0^2 - 3M\mathbf{r}_0 - 2a^2) \quad (\text{A9})$$

$$B \equiv -\frac{6\mu M\Delta}{(m_1 + m_2)\mathbf{r}_0^4 F_\sigma^2(\mathbf{r}_0)} (\sigma\sqrt{M\mathbf{r}_0} - a). \quad (\text{A10})$$

We also rewrite the equation for $\theta_{(1)}$ as

$$\frac{d^2\theta_{(1)}}{d\tau^2} + k_\theta^2\theta_{(1)} + B\dot{y}z = 0, \quad (\text{A11})$$

where

$$k_\theta^2 \equiv \frac{M}{\mathbf{r}_0^3 F_\sigma^2(\mathbf{r}_0)} (\mathbf{r}_0^2 + 3a^2 - 4a\sigma\sqrt{M\mathbf{r}_0}). \quad (\text{A12})$$

We find that $k_r^2 > 0$ and $k_\theta^2 > 0$ when $\mathbf{r}_0 > \mathbf{r}_{\text{ISCO}}$, which guarantees stability against homogeneous perturbations. This fact is consistent with the stability of a circular geodesic. In order to understand the oscillations of the deviation $\mathbf{r}_{(1)}$ and $\theta_{(1)}$, we expand the oscillation frequencies k_r^2 and k_θ^2 in the limit of $M/\mathbf{r}_0 \ll 1$ as

$$k_r \approx \frac{M^{1/2}}{\mathbf{r}_0^{3/2}} \left[1 - \frac{3M}{2\mathbf{r}_0} + \frac{3a\sigma}{\mathbf{r}_0} \sqrt{\frac{M}{\mathbf{r}_0}} \right] = \mathfrak{w}_R - \mathfrak{w}_{\text{dS}} - \tilde{\mathfrak{w}}_{\text{LT}},$$

$$k_\theta \approx \frac{M^{1/2}}{\mathbf{r}_0^{3/2}} \left[1 + \frac{3M}{2\mathbf{r}_0} - \frac{3a\sigma}{\mathbf{r}_0} \sqrt{\frac{M}{\mathbf{r}_0}} \right] = \mathfrak{w}_R + \mathfrak{w}_{\text{dS}} + \tilde{\mathfrak{w}}_{\text{LT}},$$

where $\tilde{\mathfrak{w}}_{\text{LT}} = -3Ma\sigma/\mathbf{r}_0^3$. The meaning of the $\theta_{(1)}$ oscillations is more clear since it describes the deviation from the equatorial plane. There are three origins of the oscillations; one is the angular frequency of the rotating frame, the second is caused by the de Sitter precession, and the third is related to the Lense-Thirring precession between the rotation of the c.m. and the BH spin, which is slightly different from that of a binary angular momentum and the BH spin [35,36].

Including the inhomogeneous perturbations caused by a binary motion, we find formally general solutions for Eqs. (A7) and (A11) as

$$\mathbf{r}_{(1)} = a_r \cos[k_r\tau] + b_r \sin[k_r\tau] - \frac{1}{k_r} \int_0^\tau d\tau' [A(x(\tau')^2 - z(\tau')^2) + B\dot{y}(\tau')x(\tau')] \times \sin[k_r(\tau - \tau')], \quad (\text{A13})$$

$$\theta_{(1)} = a_\theta \cos[k_\theta\tau] + b_\theta \sin[k_\theta\tau] - \frac{B}{k_\theta} \int_0^\tau d\tau' \dot{y}(\tau')z(\tau') \sin[k_\theta(\tau - \tau')], \quad (\text{A14})$$

where $a_r, b_r, a_\theta,$ and b_θ are arbitrary constants, which are determined by initial conditions. Since $\dot{y}x$ and $\dot{y}z$ may oscillate around zero, the integration with those terms may not induce instability. On the other hand, the integration with $(x^2 - z^2)$ does not have definite sign. We have to check its stability numerically by use of numerical solution of a binary motion.

In Figs. 12 and 13, we show the time evolution of $\mathbf{r}_{(1)}$ and $\theta_{(1)}$ for Model I ($a = 0.9M, \mathbf{r}_0 = 10M,$ and $\mathbf{a}_0 = 0.005M$) and Model III ($a = 0.9M, \mathbf{r}_0 = 3.2M,$ and $\mathbf{a}_0 = 0.005M$). We assume that the initial values of $\mathbf{r}_{(1)}$ and $\theta_{(1)}$ and their time derivatives vanish.

Since Model I shows a regular vZLK oscillation, from Fig. 12, we find good correlation between the eccentricity and the deviations from a circular orbit. $\mathbf{r}_{(1)}$ oscillates around small nonzero positive value with small amplitude. The oscillation center slightly increases when the eccentricity becomes large, but the oscillation amplitude does not change. For $\theta_{(1)}$, the oscillation center is almost zero, and

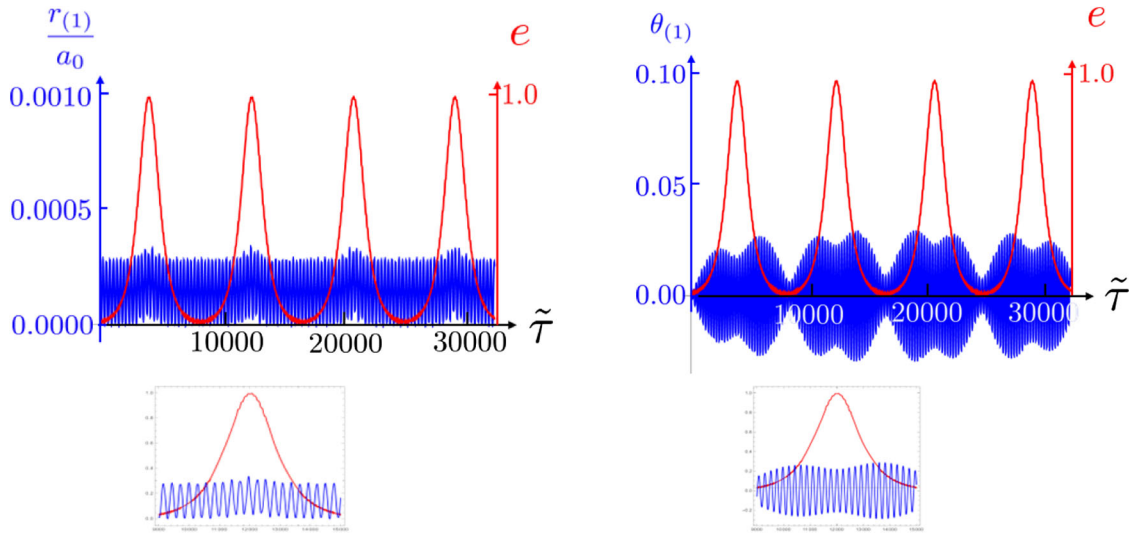


FIG. 12. The time evolution of $\mathbf{r}_{(1)}$ (left) and $\theta_{(1)}$ (right) for Model I ($a = 0.9M, \mathbf{r}_0 = 10M,$ and $\mathbf{a}_0 = 0.005M$). The bottom figures show the enlargement of the period of $\tilde{\tau} = 9000\text{--}15000$. We also show the evolution of the eccentricity (red curves) to see the correlation.

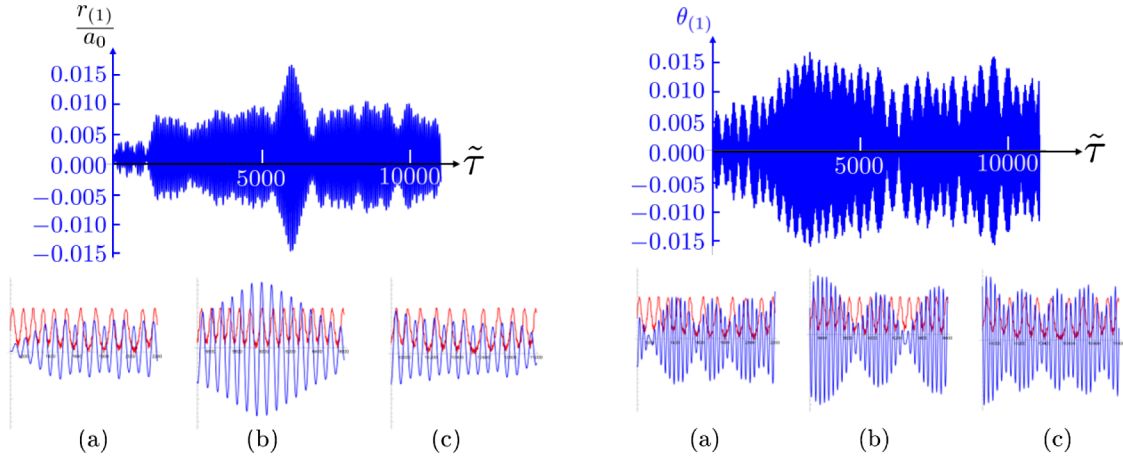


FIG. 13. The time evolution of $\mathbf{r}_{(1)}$ (left) and $\theta_{(1)}$ (right) for the model with $a = 0.9M$, $\mathbf{r}_0 = 3.2M$, and $\mathbf{a}_0 = 0.005M$. The bottom figures (a), (b), and (c) depict the first tenth, the middle tenth and the last tenth of the period, respectively. We show the evolution of the eccentricity (e) and the deviations $[\mathbf{r}_{(1)}, \theta_{(1)}]$.

oscillation amplitude changes in time. Although there is no correlation with the eccentricity, the oscillation pattern is periodic and the period is the same as that of the vZLK oscillations. Note that the oscillation amplitude in the radial direction $[|\mathbf{r}_{(1)}| \sim 10^{-4}]$ is much smaller than that in the θ direction $[|\theta_{(1)}| \sim 10^{-2}]$.

For Model III (Fig. 13), the binary system is close to the chaotic boundary. In this chaotic vZLK oscillation model, we find the motion of the c.m. also becomes irregular. There is no correlation between the evolution of the eccentricity (red curves) and the oscillations of $\mathbf{r}_{(1)}$ and $\theta_{(1)}$ (blue curves), as shown in the bottom figures of 13. The oscillation amplitudes of the radial direction and θ direction are almost the same in this chaotic case $[|\mathbf{r}_{(1)}| \sim |\theta_{(1)}| \sim 10^{-2}]$.

APPENDIX B: LAGRANGE PLANETARY EQUATIONS FOR A BINARY SYSTEM NEAR SMBH

To comprehend our numerical findings better, we should consider the Lagrange planetary equations. These equations provide the evolution of orbital parameters, such as the semimajor axis, eccentricity, and inclination. To derive these planetary equations, we work with the proper Hamiltonian, where the mass parameter is set to $\mu = 1$. The proper Hamiltonian is defined as follows:

$$\bar{\mathcal{H}} = \bar{\mathcal{H}}_0 + \bar{\mathcal{H}}_1,$$

where

$$\bar{\mathcal{H}}_0 = \frac{1}{2} \bar{\mathbf{p}}^2 - \frac{G(m_1 + m_2)}{r},$$

$$\bar{\mathcal{H}}_1 = \sigma \mathfrak{w}_P (\bar{\rho}_y \mathbf{x} - \bar{\rho}_x \mathbf{y}) + \frac{M}{2\mathbf{r}_0^3} \left[r^2 + \frac{3}{F_\sigma^2(\mathbf{r}_0)} (-\Delta(\mathbf{r}_0) (\mathbf{x} \cos \sigma \mathfrak{w}_R \tau - \mathbf{y} \sin \sigma \mathfrak{w}_R \tau)^2 + (\sigma \sqrt{M \mathbf{r}_0} - a)^2 z^2) \right].$$

The position $\mathbf{r} = (x, y, z)$ of a binary should be described in the nonrotating proper reference frame.

The unperturbed Hamiltonian, denoted as $\bar{\mathcal{H}}_0$, is equivalent to that of a binary system in Newtonian dynamics. It leads to an elliptical orbit, described by the equation

$$\mathbf{r} = \frac{\mathbf{a}(1 - e^2)}{1 + e \cos f}, \quad (\text{B1})$$

Here, r represents the radial distance from the c.m., while a , e , and f are the semimajor axis, eccentricity, and true anomaly, respectively. This orbital plane is inclined at an

angle I relative to the equatorial plane in the proper reference frame. Consequently, the relative position vector $\mathbf{r} = (x, y, z)$ of the binary system can be determined by the orbital parameters $(\omega, \Omega, \mathbf{a}, e, I, f)$ as described in Eq. (4.11) with Eq. (B1). The introduction of Delaunay variables further refines this description as follows:

$$\begin{cases} \mathfrak{L} = n(t - t_0) \\ \mathfrak{g} = \omega \\ \mathfrak{h} = \Omega \end{cases} \quad \text{and} \quad \begin{cases} \mathfrak{Q} = \sqrt{G(m_1 + m_2)} \mathbf{a} \\ \mathfrak{G} = \sqrt{G(m_1 + m_2)} \mathbf{a} (1 - e^2) \\ \mathfrak{S} = \sqrt{G(m_1 + m_2)} \mathbf{a} (1 - e^2) \cos I, \end{cases}$$

where

$$n \equiv \frac{2\pi}{P} = \sqrt{\frac{G(m_1 + m_2)}{a^3}},$$

is the mean motion, we find new unperturbed Hamiltonian as

$$\tilde{\mathcal{H}}_0 = -\frac{G^2(m_1 + m_2)^2}{2\mathcal{Q}^2}.$$

Including the perturbations $\tilde{\mathcal{H}}_1$, we obtain the Hamiltonian for the Delaunay variables as

$$\tilde{\mathcal{H}} = \tilde{\mathcal{H}}_0 + \tilde{\mathcal{H}}_1.$$

The proper Hamiltonian is described by the orbital parameters by inserting the relation given in Eq. (4.11) with Eq. (B1). We then find the perturbed Hamiltonian as

$$\tilde{\mathcal{H}}_1 = \tilde{\mathcal{H}}_{1-P} + \tilde{\mathcal{H}}_{1-\bar{R}},$$

where

$$\tilde{\mathcal{H}}_{1-P} = \sigma \mathfrak{m}_P r^2(\mathbf{a}, e, f) \{n \cos I (1 - e^2)^{-3/2} (1 + e \cos f)^2 - \mathfrak{m}_P (\cos^2(\omega + f) + \sin^2(\omega + f) \cos^2 I)\}, \quad (\text{B2})$$

$$\begin{aligned} \tilde{\mathcal{H}}_{1-\bar{R}} = & \frac{M}{2\mathbf{r}_0^3} r^2(\mathbf{a}, e, f) \left\{ 1 - \frac{3\Delta(\mathbf{r}_0)}{F_\sigma^2(\mathbf{r}_0)} [\cos(\Omega + \sigma \mathfrak{m}_R \tau) \cos(\omega + f) - \sin(\Omega + \sigma \mathfrak{m}_R \tau) \sin(\omega + f) \cos I]^2 \right. \\ & \left. + \frac{3(\sigma \sqrt{M \mathbf{r}_0} - a)^2}{F_\sigma^2(\mathbf{r}_0)} \sin^2(\omega + f) \sin^2 I \right\}. \end{aligned} \quad (\text{B3})$$

We then obtain the planetary equations for the present hierarchical triple system, which is mathematically equivalent to our basic equations in the text.

1. Double-averaging approach

Rather than directly solving the Lagrange planetary equations, our approach involves averaging the perturbed Hamiltonian over two periods; the inner and outer orbital periods. This allows us to simplify the equations for analysis. We are interested in understanding the long-term behavior of the system, particularly phenomena like the vZLK mechanism.

The doubly-averaged Hamiltonian is defined by

$$\langle\langle \tilde{\mathcal{H}}_1 \rangle\rangle \equiv \frac{1}{2\pi} \int_0^{2\pi} d\mathcal{I}_{\text{out}} \left(\frac{1}{2\pi} \int_0^{2\pi} d\mathcal{I} \tilde{\mathcal{H}}_1 \right)$$

Since the outer orbit is circular, we find that $\mathcal{I}_{\text{out}} = f_{\text{out}} = \mathfrak{m}_0 \tau$. We also have

$$d\mathcal{I} = \frac{1}{\sqrt{1 - e^2}} \left(\frac{r}{a} \right)^2 df.$$

Inserting Eqs. (B2) and (B3) into the above integrals, we find the doubly-averaged Hamiltonian as

$$\begin{aligned} \langle\langle \tilde{\mathcal{H}}_1 \rangle\rangle = & \sigma \mathfrak{m}_P n a^2 \sqrt{1 - e^2} \cos I - \frac{a^2}{8} \left\{ (2 + 3e^2) \left[\mathfrak{m}_P^2 (3 + \cos 2I) + \frac{M(\mathbf{r}_0^2 + 3a^2 - 4a\sigma\sqrt{M\mathbf{r}_0})}{4F_\sigma^2(\mathbf{r}_0)\mathbf{r}_0^3} (1 + 3\cos 2I) \right] \right. \\ & \left. + 10e^2 \sin^2 I \cos 2\omega \left[\mathfrak{m}_P^2 + \frac{3M(\mathbf{r}_0^2 + 3a^2 - 4a\sigma\sqrt{M\mathbf{r}_0})}{4F_\sigma^2(\mathbf{r}_0)\mathbf{r}_0^3} \right] \right\}. \end{aligned} \quad (\text{B4})$$

Using the double-averaged Hamiltonian Eq. (B4), we obtain the double-averaged Lagrange planetary equations as

$$\dot{e} = \frac{5}{4} \left(\mathfrak{m}_P^2 + \frac{3M(\mathbf{r}_0^2 + 3a^2 - 4a\sigma\sqrt{M\mathbf{r}_0})}{4F_\sigma^2(\mathbf{r}_0)\mathbf{r}_0^3} \right) \frac{e\sqrt{1 - e^2}}{n} (1 - \cos 2I) \sin 2\omega, \quad (\text{B5})$$

$$\dot{I} = -\frac{5}{4} \left(\mathfrak{m}_P^2 + \frac{3M(\mathbf{r}_0^2 + 3a^2 - 4a\sigma\sqrt{M\mathbf{r}_0})}{4F_\sigma^2(\mathbf{r}_0)\mathbf{r}_0^3} \right) \frac{e^2}{n\sqrt{1 - e^2}} \sin 2I \sin 2\omega, \quad (\text{B6})$$

$$\begin{aligned} \dot{\omega} = & \frac{1}{4n} \left(\mathfrak{w}_p^2 + \frac{3M(\mathbf{r}_0^2 + 3a^2 - 4a\sigma\sqrt{M\mathbf{r}_0})}{4F_\sigma^2(\mathbf{r}_0)\mathbf{r}_0^3} \right) [\sqrt{1-e^2}[3 + 5\cos 2I + 5(1-\cos 2I)\cos 2\omega] \\ & + \frac{5e^2}{\sqrt{1-e^2}}(1 + \cos 2I)(1 - \cos 2\omega)] + \frac{2\sqrt{1-e^2}}{n} \mathfrak{w}_p^2, \end{aligned} \quad (\text{B7})$$

$$\dot{\Omega} = \sigma \mathfrak{w}_p + \frac{\cos I}{2n\sqrt{1-e^2}} \left(\mathfrak{w}_p^2 + \frac{3M(\mathbf{r}_0^2 + 3a^2 - 4a\sigma\sqrt{M\mathbf{r}_0})}{4F_\sigma^2(\mathbf{r}_0)\mathbf{r}_0^3} \right) [-(2 + 3e^2) + 5e^2 \cos 2\omega]. \quad (\text{B8})$$

The semimajor axis \mathbf{a} is constant in the present approximation. Also, from Eqs. (B5) and (B6), we can easily check the conservation equation such that

$$\frac{d}{d\tau}(\sqrt{1-e^2} \cos I) = 0,$$

which corresponds to conservation of the z-component of the angular momentum.

2. vZLK oscillations

Introducing a ‘‘potential’’ by $V_S \equiv -\langle\langle \tilde{\mathcal{H}}_1 \rangle\rangle$, we rewrite the above planetary equations as

$$\dot{e} = -\frac{\sqrt{1-e^2}}{na^2 e} \frac{\partial V_S}{\partial \omega}, \quad (\text{B9})$$

$$\dot{I} = \frac{\cos I}{na^2 \sin I \sqrt{1-e^2}} \frac{\partial V_S}{\partial \omega}, \quad (\text{B10})$$

$$\dot{\omega} = \frac{\sqrt{1-e^2}}{na^2 e} \frac{\partial V_S}{\partial e} - \frac{\cos I}{na^2 \sin I \sqrt{1-e^2}} \frac{\partial V_S}{\partial I}, \quad (\text{B11})$$

$$\dot{\Omega} = \frac{1}{na^2 \sin I \sqrt{1-e^2}} \frac{\partial V_S}{\partial I}. \quad (\text{B12})$$

We derive closed-form differential equations for the variables e , I , and ω using Eqs. (B9), (B10), and (B11). These equations provide insights into various properties of vZLK oscillations, including the oscillation amplitude of eccentricity and the oscillation timescale. This analysis is consistent with previous studies on Newtonian and 1 PN hierarchical triple systems, as discussed in [34].

The potential is written by use of $\eta \equiv \sqrt{1-e^2}$ and $\mu_I \equiv \cos I$ as

$$\begin{aligned} V_S & \equiv -\langle\langle \tilde{\mathcal{H}}_1 \rangle\rangle \\ & = \frac{\mathbf{a}^2 M(\mathbf{r}_0^2 + 3a^2 - 4a\sigma\sqrt{M\mathbf{r}_0})}{16F_\sigma^2(\mathbf{r}_0)\mathbf{r}_0^3} v_S(\eta, \mu_I), \end{aligned}$$

where

$$\begin{aligned} v_S(\eta, \mu_I) & \equiv 2(-1 + 3\mu_I^2 \eta^2)(1 + \alpha_p) + 12C_{\text{vZLK}} \\ & + 4\alpha_p \left(2 - \frac{3\sigma n}{\mathfrak{w}_p} \mu_I \eta \right), \end{aligned}$$

with

$$\alpha_p \equiv \frac{4\mathfrak{w}_p^2 F_\sigma^2(\mathbf{r}_0)\mathbf{r}_0^3}{3M(\mathbf{r}_0^2 + 3a^2 - 4a\sigma\sqrt{M\mathbf{r}_0})},$$

$$C_{\text{vZLK}} \equiv (1 - \eta^2) \left[(1 + 2\alpha_p) - \frac{5}{2}(1 + \alpha_p)(1 - \mu_I^2) \sin^2 \omega \right].$$

Note that when $\alpha_p = 0$, we find the same equations for Newtonian hierarchical triple system with quadrupole approximation. The terms with α_p give relativistic corrections.

Introducing the normalized time $\tilde{\tau}$, which is defined by

$$\tilde{\tau} \equiv \frac{\tau}{\tau_{\text{vZLK}}},$$

with the typical vZLK timescale

$$\tau_{\text{vZLK}} \equiv \frac{16nF_\sigma^2(\mathbf{r}_0)\mathbf{r}_0^3}{M(\mathbf{r}_0^2 + 3a^2 - 4a\sigma\sqrt{M\mathbf{r}_0})},$$

the above planetary equation is rewritten as

$$\begin{aligned} \frac{d\eta}{d\tilde{\tau}} & = \frac{\partial v_S}{\partial \omega}, \\ \frac{1}{\mu_I} \frac{d\mu_I}{d\tilde{\tau}} & = -\frac{1}{\eta} \frac{\partial v_S}{\partial \omega}, \\ \frac{d\omega}{d\tilde{\tau}} & = -\frac{\partial v_S}{\partial \eta} + \frac{\mu_I}{\eta} \frac{\partial v_S}{\partial \mu_I}. \end{aligned}$$

From these equations, we can easily show that

$$\frac{d(\mu_I \eta)}{d\tilde{\tau}} = 0, \quad \frac{dv_S}{d\tilde{\tau}} = 0,$$

which means there exist two conserved quantities $\vartheta \equiv \mu_I \eta$ and C_{vZLK} just as the Newtonian and 1 PN hierarchical triple system under dipole approximation. Using these two conserved quantities, we obtain a single equation for η as

$$\frac{d\eta^2}{d\tilde{\tau}} = -24\sqrt{2}\sqrt{f(\eta^2)g(\eta^2)},$$

with

$$\xi_0 = 1 - \frac{C_{\text{vZLK}}}{1 + 2\alpha_{\text{p}}},$$

$$\xi_{\pm} = \frac{1}{2} \left[\left(1 + \frac{5(1 + \alpha_{\text{p}})}{3 + \alpha_{\text{p}}} \vartheta^2 + \frac{2}{3 + \alpha_{\text{p}}} C_{\text{vZLK}} \right) \pm \sqrt{\left(1 + \frac{5(1 + \alpha_{\text{p}})}{3 + \alpha_{\text{p}}} \vartheta^2 + \frac{2}{3 + \alpha_{\text{p}}} C_{\text{vZLK}} \right)^2 - \frac{20(1 + \alpha_{\text{p}})}{3 + \alpha_{\text{p}}} \vartheta^2} \right],$$

are the solutions of $f(\xi) = 0$ and $g(\xi) = 0$, respectively.

We can find the relativistic corrections with α_{p} , which is evaluated as

$$\alpha_{\text{p}} = \frac{4(\mathbf{r}_0 - F_{\sigma}(\mathbf{r}_0))^2}{3(\mathbf{r}_0^2 + 3a^2 - 4a\sigma\sqrt{M\mathbf{r}_0})}.$$

This constant α_{p} is small when rotation of SMBH is small (the maximum value for Schwarzschild BH is 0.11), but it can be large when SMBH is rotating rapidly and the c.m. is near the ISCO radius. For example, when $\mathbf{a} = 0.9M(0.99M)$, $\alpha_{\text{p}} \approx 0.88(5.56)$ at the ISCO radius, and it diverges as $\mathbf{a} \rightarrow M$. It is because the denominator vanishes in this limit.

Analyzing the above equation, we find that there exists vZLK oscillations in this system just the same as in Newtonian hierarchical triple system, and we can classify the vZLK oscillations by the sign of C_{vZLK} into two cases: (a) $C_{\text{vZLK}} > 0$ (rotation); (b) $C_{\text{vZLK}} < 0$ (libration).

a. $C_{\text{vZLK}} > 0$ (rotation)

In this case, $0 < \xi_- < 1 < \xi_+$ and $0 < \xi_0 < 1$. This is possible if

$$0 < C_{\text{vZLK}} < 1 + 2\alpha_{\text{p}}.$$

Hence, we find the maximum and minimum values of the eccentricity as

$$e_{\text{max}} = \sqrt{1 - \xi_-}, \quad e_{\text{min}} = \sqrt{1 - \xi_0}.$$

The vZLK oscillation timescale is given by

$$T_{\text{vZLK}} = \tau_{\text{vZLK}} \mathfrak{Z}_{\text{vZLK}}^{(\text{rot})}, \quad (\text{B13})$$

$$\begin{aligned} f(\eta^2) &\equiv (1 + 2\alpha_{\text{p}})(1 - \eta^2) - C_{\text{vZLK}}, \\ g(\eta^2) &\equiv -5(1 + \alpha_{\text{p}})\vartheta^2 - (3 + \alpha_{\text{p}})\eta^4 \\ &\quad + [5(1 + \alpha_{\text{p}})\vartheta^2 + 3 + \alpha_{\text{p}} + 2C_{\text{KvZLK}}]\eta^2. \end{aligned}$$

Setting $\xi = \eta^2$, we find

$$\frac{d\xi}{d\tilde{\tau}} = -24\sqrt{2(1 + 2\alpha_{\text{p}})(3 + \alpha_{\text{p}})}\sqrt{(\xi - \xi_0)(\xi - \xi_+)(\xi - \xi_-)},$$

where

where

$$\mathfrak{Z}_{\text{vZLK}}^{(\text{rot})} \equiv \frac{K\left(\sqrt{\frac{\xi_0 - \xi_-}{\xi_+ - \xi_-}}\right)}{6\sqrt{2(1 + 2\alpha_{\text{p}})(3 + \alpha_{\text{p}})(\xi_+ - \xi_-)}}.$$

$K(k)$ is the complete elliptic integral of the first kind with the elliptic modulus k .

b. $C_{\text{vZLK}} < 0$ (libration)

Since $0 < \xi_- < \xi_+ < 1$ and $\xi_0 < 0$ in this case, we find

$$e_{\text{max}} = \sqrt{1 - \xi_-}, \quad e_{\text{min}} = \sqrt{1 - \xi_+}.$$

It occurs when

$$-\frac{3 + \alpha_{\text{p}}}{2} < C_{\text{vZLK}} < 0,$$

and

$$\vartheta < \frac{(\sqrt{3 + \alpha_{\text{p}}} - \sqrt{-2C_{\text{vZLK}}})}{\sqrt{5(1 + \alpha_{\text{p}})}}.$$

The vZLK timescale is given by

$$T_{\text{vZLK}} = \tau_{\text{vZLK}} \mathfrak{Z}_{\text{vZLK}}^{(\text{lib})}, \quad (\text{B14})$$

where

$$\mathfrak{Z}_{\text{vZLK}}^{(\text{lib})} \equiv \frac{K\left(\sqrt{\frac{\xi_+ - \xi_-}{\xi_0 - \xi_-}}\right)}{6\sqrt{2(1+2\alpha_p)(3+\alpha_p)(\xi_0 - \xi_-)}}.$$

The maximum and minimum values of the eccentricity in the vZLK oscillations are determined by two conserved parameters, ϑ and C_{vZLK} . Note that the maximum eccentricity in vZLK oscillations is important, especially when we discuss emission of GWs.

The timescale of the vZLK oscillations is also important for observation of the gravitational waves. Since $\mathfrak{Z}_{\text{vZLK}}^{(\text{rot})}$ and $\mathfrak{Z}_{\text{vZLK}}^{(\text{lib})}$ are order of unity, the timescale is almost determined by τ_{vZLK} , which is rewritten by

$$n\tau_{\text{vZLK}} = 16f \frac{(\mathbf{r}_0^2 - 3M\mathbf{r}_0 + 2a\sigma\sqrt{M\mathbf{r}_0})}{(\mathbf{r}_0^2 + 3a^2 - 4a\sigma\sqrt{M\mathbf{r}_0})}. \quad (\text{B15})$$

Some example of the exact values of T_{vZLK} is given in Fig. 14.

We then may evaluate the relativistic effects (including de Sitter precession) by comparison with the Newtonian value $T_{\text{vZLK}}^{(\text{N})}$ as shown in Fig. 15.

Fig. 15 shows that the relativistic effects reduce the vZLK timescale by a factor 0.1–0.25. Although the ratio vanishes at the ISCO radius in the limit of $a \rightarrow M$, the double-averaging approximation is no longer valid in this limit.

c. Critical inclination angle

We can also evaluate a critical inclination angle, beyond which the vZLK oscillation occurs even when the initial eccentricity is very small. It is given by the condition for a bifurcation point with $C_{\text{vZLK}} = 0$ with $\omega = 90^\circ$. Setting

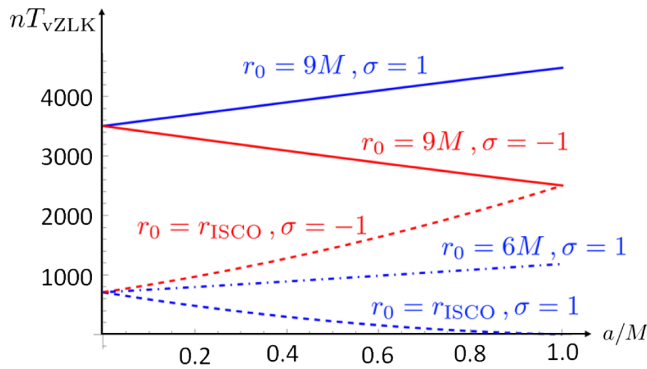


FIG. 14. The period of vZLK oscillations T_{vZLK} is shown in terms of the Kerr rotation parameter a . The blue and red curves correspond to the prograde ($\sigma = 1$) and retrograde ($\sigma = -1$) orbits. The solid curves show the case of $\mathbf{r}_0 = 9M$, while the dot-dashed one and dashed ones are $\mathbf{r}_0 = 6M$ and $\mathbf{r}_0 = r_{\text{ISCO}}$, respectively. The semimajor axis is chosen as $\mathbf{a} = 0.005M$.

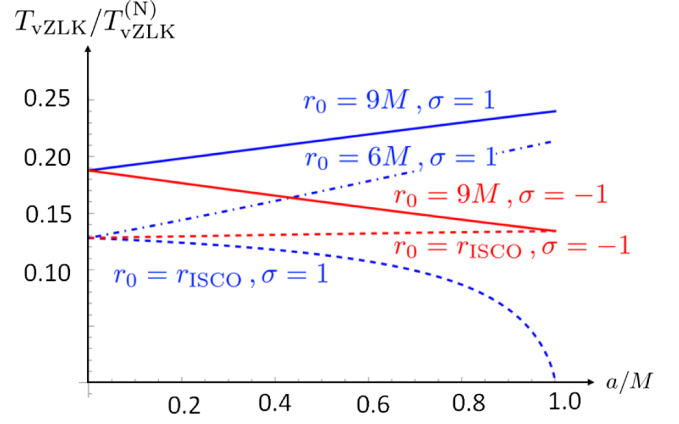


FIG. 15. The ratio of vZLK oscillation period T_{vZLK} to its Newtonian value is shown in terms of the Kerr rotation parameter a . The colors and types of the curves are the same as those in Fig. 14. The semimajor axis is chosen as $\mathbf{a} = 0.005M$.

$$(1 + 2\alpha_p) - \frac{5}{2}(1 + \alpha_p) \sin^2 I_{\text{crit}} = 0,$$

we obtain

$$I_{\text{crit}} = \sin^{-1} \sqrt{\frac{2(1 + 2\alpha_p)}{5(1 + \alpha_p)}}.$$

We find that the critical inclination angle changes from 63.4° ($a = M$) [41.6° ($a = 0$)] to the Newtonian value $I_{\text{crit}}^{(\text{N})} = \sin^{-1} \sqrt{2/5} \approx 39.2^\circ$ as \mathbf{r}_0 increases from the ISCO radius to infinity. However the critical value depends on the orbital parameters, especially on \mathbf{r}_0 and \mathbf{a}_0 . Assuming

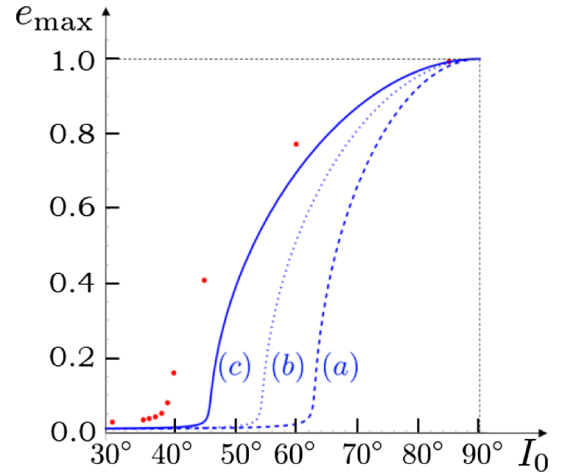


FIG. 16. The maximum values of the eccentricity in vZLK oscillations based on the double-averaging approximation: (a) $C_{\text{chaotic}} = 1$ (the dashed curve), (b) $C_{\text{chaotic}} = 3$ (the dotted curve), (c) $C_{\text{chaotic}} = 5$ (the solid curve). We choose $\mathbf{r}_0 = r_{\text{ISCO}}$ and $a = 0.999M$. The red dots denote the result obtained by the direct integration of the equations of motion.

$a = 0.999M$, $r_0 = r_{\text{ISCO}}$, and $e_0 = 0.01$, we evaluate the maximum value of the eccentricity in vZLK oscillations, which is given in Fig. 16. In the case of $C_{\text{chaotic}} = 1$, which corresponds to the firmness parameter $\mathfrak{f} = 1$, the critical inclination angle is slightly larger than 60° . However, this model suffers from chaotic instability. As we discussed in

the text, stability against chaotic perturbations must satisfy $C_{\text{chaotic}} \lesssim 3-4$. In that case, the critical inclination angle becomes smaller as $40^\circ-50^\circ$. The red dots denote the result obtained by the direct integration of the equations of motion, which shows that the true critical inclination angle is about 40° even for $a = 0.999M$.

-
- [1] B. P. Abbott, R. Abbott, T. D. Abbott, S. Abraham, F. Acernese, K. Ackley, C. Adams, V. B. Adya, C. Affeldt *et al.*, *Living Rev. Relativity* **23** (2020).
- [2] B. P. Abbott, R. Abbott, T. D. Abbott, S. Abraham, F. Acernese, K. Ackley, C. Adams, V. B. Adya, C. Affeldt *et al.*, *SoftwareX* **13**, 100658 (2021).
- [3] B. P. Abbott *et al.* (LIGO Scientific and Virgo Collaborations), *Phys. Rev. Lett.* **116**, 061102 (2016).
- [4] B. P. Abbott *et al.* (LIGO Scientific and Virgo Collaborations), *Phys. Rev. Lett.* **119**, 161101 (2017).
- [5] B. P. Abbott *et al.* (LIGO Scientific and Virgo Collaborations), *Phys. Rev. D* **100**, 104036 (2019).
- [6] The LIGO Scientific and Virgo Collaborations, *Astrophys. J.* **900**, L13 (2020).
- [7] The LIGO Scientific and Virgo Collaborations, *Phys. Rev. D* **103**, 104027 (2021).
- [8] The LIGO Scientific and Virgo Collaborations, *Astrophys. J. Lett.* **913**, L7 (2021).
- [9] The LIGO Scientific, the Virgo, and the KAGRA Collaborations, *Astrophys. J.* **949**, 76 (2023).
- [10] M. A. S. Martinez, G. Fragione, K. Kremer, S. Chatterjee, C. L. Rodriguez, J. Samsing, C. S. Ye, N. C. Weatherford, M. Zevin, S. Naoz *et al.*, *Astrophys. J.* **903**, 67 (2020).
- [11] D. Gerosa and M. Fishbach, *Nat. Astron.* **5**, 749 (2021).
- [12] D. C. Heggie, *Mon. Not. R. Astron. Soc.* **173**, 729 (1975).
- [13] P. Hut, *Astrophys. J.* **403**, 256 (1993).
- [14] J. Samsing, M. MacLeod, and E. Ramirez-Ruiz, *Astrophys. J.* **784**, 71 (2014).
- [15] R. L. Riddle *et al.*, *Astrophys. J.* **799**, 4 (2015).
- [16] F. Antonini, S. Chatterjee, C. Rodriguez, M. Morscher, B. Pattabiraman, V. Kalogera, and F. Rasio, *Astrophys. J.* **816**, 2 (2016).
- [17] A. P. Stephan, S. Naoz, A. M. Ghez, M. R. Morris, A. Ciurlo, T. Do, K. Breivik, S. Coughlin, and C. L. Rodriguez, *Astrophys. J.* **878**, 58 (2019).
- [18] M. Mapelli, F. Santoliquido, Y. Bouffanais, M. Arca Sedda, M. C. Artale, and A. Ballone, *Symmetry* **13**, 1678 (2021).
- [19] V. Gayathri, I. Bartos, Z. Haiman, S. Klimentko, B. Kocsis, S. Márka, and Y. Yang, *Astrophys. J.* **890**, L20 (2020).
- [20] H. von Zeipel, *Astron. Nachr.* **183**, 345 (1910).
- [21] M. Lidov, *Planet. Space Sci.* **9**, 719 (1962).
- [22] Y. Kozai, *Astron. J.* **67**, 591 (1962).
- [23] I. Shevchenko, *The Lidov-Kozai Effect—Applications in Exoplanet Research and Dynamical Astronomy* (Springer, New York, 2017).
- [24] C. Kimball, C. Talbot, C. P. L. Berry, M. Zevin, E. Thrane, V. Kalogera, R. Buscicchio, M. Carney, T. Dent, H. Middleton *et al.*, *Astrophys. J. Lett.* **915**, L35 (2021).
- [25] S. Naoz, B. Kocsis, A. Loeb, and N. Yunes, *Astrophys. J.* **773**, 187 (2013).
- [26] S. Naoz, W. Farr, and F. Rasio, *Astrophys. J.* **754**, L36 (2012).
- [27] S. Naoz, *Annu. Rev. Astron. Astrophys.* **54**, 441 (2016).
- [28] S. Naoz, C. M. Will, E. Ramirez-Ruiz, A. Hees, A. M. Ghez, and T. Do, *Astrophys. J.* **888**, L8 (2019).
- [29] J. Teyssandier, S. Naoz, I. Lizarraga, and F. A. Rasio, *Astrophys. J.* **779**, 169 (2013).
- [30] G. Li, S. Naoz, B. Kocsis, and A. Loeb, *Mon. Not. R. Astron. Soc.* **451**, 1341 (2015).
- [31] C. Will, *Phys. Rev. D* **89**, 044043 (2014).
- [32] C. Will, *Classical Quantum Gravity* **31**, 244001 (2014).
- [33] H. Suzuki, P. Gupta, H. Okawa, and K. Maeda, *Mon. Not. R. Astron. Soc.* **486**, L52 (2019).
- [34] H. Suzuki, P. Gupta, H. Okawa, and K. Maeda, *Mon. Not. R. Astron. Soc.* **500**, 1645 (2020).
- [35] B. Liu, D. Lai, and Y.-H. Wang, *Astrophys. J. Lett.* **883**, L7 (2019).
- [36] B. Liu and D. Lai, *Astrophys. J.* **924**, 127 (2022).
- [37] H. Lim and C. L. Rodriguez, *Phys. Rev. D* **102**, 064033 (2020).
- [38] Y. Fang and Q.-G. Huang, *Phys. Rev. D* **99**, 012014 (2019).
- [39] Y. Fang, X. Chen, and Q.-G. Huang, *Astrophys. J.* **887**, 210 (2019).
- [40] P. Amaro-Seoane, A. Sesana, L. Hoffman, M. Benacquista, C. Eichhorn, J. Makino, and R. Spurzem, *Mon. Not. R. Astron. Soc.* **402**, 2308 (2010).
- [41] F. Antonini and H. Perets, *Astrophys. J.* **757**, 27 (2012).
- [42] B. Hoang, S. Naoz, B. Kocsis, F. A. Rasio, and F. Dosopoulou, *Astrophys. J.* **856**, 140 (2018).
- [43] F. Antonini, S. Chatterjee, C. Rodriguez, M. Morscher, and B. Pattabiraman, *Astrophys. J.* **816**, 2 (2016).
- [44] Y. Meiron, B. Kocsis, and A. Loeb, *Astrophys. J.* **834**, 2 (2017).
- [45] T. Robson, N. Cornish, N. Tamanini, and S. Toonen, *Phys. Rev. D* **98**, 064012 (2018).
- [46] L. Randall and Z.-Z. Xianyu, *Astrophys. J.* **878**, 75 (2019).
- [47] L. Randall and Z.-Z. Xianyu, arXiv:1902.08604.
- [48] B.-M. Hoang, S. Naoz, B. Kocsis, W. M. Farr, and J. McIver, *Astrophys. J. Lett.* **875**, L31 (2019).
- [49] R. Emami and A. Loeb, *Mon. Not. R. Astron. Soc.* **495**, 536 (2020).
- [50] P. Gupta, H. Suzuki, H. Okawa, and K. Maeda, *Phys. Rev. D* **101**, 104053 (2020).

- [51] A. Kuntz and K. Leyde, *Phys. Rev. D* **108**, 024002 (2023).
- [52] F. K. Manasse and C. W. Misner, *J. Math. Phys. (N.Y.)* **4**, 735 (1963).
- [53] A. I. Nesterov, *Classical Quantum Gravity* **16**, 465 (1999).
- [54] P. Delva and M. C. Angonin, *Gen. Relativ. Gravit.* **44**, 1 (2012).
- [55] P. Banerjee, S. Paul, R. Shaikh, and T. Sarkar, *Phys. Lett. B* **795**, 29 (2019).
- [56] M. Ishii, M. Shibata, and Y. Mino, *Phys. Rev. D* **71**, 044017 (2005).
- [57] R. M. Cheng and C. R. Evans, *Phys. Rev. D* **87**, 104010 (2013).
- [58] A. Kuntz, F. Serra, and E. Trincherini, *Phys. Rev. D* **104**, 024016 (2021).
- [59] A. Gorbatsievich and A. Bobrik, *AIP Conf. Proc.* **1205**, 87 (2010).
- [60] X. Chen and Z. Zhang, *Phys. Rev. D* **106**, 103040 (2022).
- [61] F. Camilloni, G. Grignani, T. Harmark, R. Oliveri, M. Orselli, and D. Pica, *Phys. Rev. D* **107**, 084011 (2023).
- [62] K. Maeda, P. Gupta, and H. Okawa, *Phys. Rev. D* **107**, 124039 (2023).
- [63] C. W. Misner, K. S. Thorne, and J. A. Wheeler, *Gravitation* (San Francisco: W.H. Freeman and Co., 1973).
- [64] M. Mathisson, *Acta Phys. Pol.* **6**, 218 (1937).
- [65] A. Papapetrou, *Proc. R. Soc. A* **209**, 248 (1951).
- [66] W. Dixon, *Phil. Trans. R. Soc. A* **277**, 59 (1974).
- [67] J. M. Bardeen, W. H. Press, and S. A. Teukolsky, *Phys. Rev. D* **107**, 124039 (2023).
- [68] C. M. Will, *Classical Quantum Gravity* **36**, 195013 (2019).
- [69] R. A. Mardling and S. J. Aarseth, *Mon. Not. R. Astron. Soc.* **321**, 398 (2001).
- [70] A. Mylläri, M. Valtonen, A. Pasechnik, and S. Mikkola, *Mon. Not. R. Astron. Soc.* **476**, 830 (2018).
- [71] S. Naoz, *Annu. Rev. Astron. Astrophys.* **54**, 441 (2016).
- [72] Y. Lithwick and S. Naoz, *Astrophys. J.* **742**, 94 (2011).
- [73] B. Katz, S. Dong, and R. Malhotra, *Phys. Rev. Lett.* **107**, 181101 (2011).
- [74] S. Naoz, W. M. Farr, Y. Lithwick, F. A. Rasio, and J. Teyssandier, *Mon. Not. R. Astron. Soc.* **431**, 2155 (2013).
- [75] G. Li, S. Naoz, B. Kocsis, and A. Loeb, *Astrophys. J.* **785**, 116 (2014).
- [76] B. Liu, D. J. Muñoz, and D. Lai, *Mon. Not. R. Astron. Soc.* **447**, 747 (2015).
- [77] V. Cardoso, F. Duque, and G. Khanna, *Phys. Rev. D* **103**, L081501 (2021).